

# SCIENTIFIC REPORTS



OPEN

## Drought rapidly diminishes the large net CO<sub>2</sub> uptake in 2011 over semi-arid Australia

Received: 26 July 2016  
Accepted: 01 November 2016  
Published: 25 November 2016

Xuanlong Ma<sup>1</sup>, Alfredo Huete<sup>1</sup>, James Cleverly<sup>2</sup>, Derek Eamus<sup>2</sup>, Frédéric Chevallier<sup>3</sup>, Joanna Joiner<sup>4</sup>, Benjamin Poulter<sup>5</sup>, Yongguang Zhang<sup>6,7</sup>, Luis Guanter<sup>8</sup>, Wayne Meyer<sup>9</sup>, Zunyi Xie<sup>1</sup> & Guillermo Ponce-Campos<sup>10</sup>

Each year, terrestrial ecosystems absorb more than a quarter of the anthropogenic carbon emissions, termed as land carbon sink. An exceptionally large land carbon sink anomaly was recorded in 2011, of which more than half was attributed to Australia. However, the persistence and spatial attribution of this carbon sink remain largely unknown. Here we conducted an observation-based study to characterize the Australian land carbon sink through the novel coupling of satellite retrievals of atmospheric CO<sub>2</sub> and photosynthesis and *in-situ* flux tower measures. We show the 2010–11 carbon sink was primarily ascribed to savannas and grasslands. When all biomes were normalized by rainfall, shrublands however, were most efficient in absorbing carbon. We found the 2010–11 net CO<sub>2</sub> uptake was highly transient with rapid dissipation through drought. The size of the 2010–11 carbon sink over Australia (0.97 Pg) was reduced to 0.48 Pg in 2011–12, and was nearly eliminated in 2012–13 (0.08 Pg). We further report evidence of an earlier 2000–01 large net CO<sub>2</sub> uptake, demonstrating a repetitive nature of this land carbon sink. Given a significant increasing trend in extreme wet year precipitation over Australia, we suggest that carbon sink episodes will exert greater future impacts on global carbon cycle.

Since the beginning of the industrial age, human activities (fossil fuel combustion, land use change, etc.) have driven the atmospheric CO<sub>2</sub> concentration from about 280 parts per million (ppm) in around 1780 to over 400 ppm in 2015<sup>1,2</sup>. The burning of fossil fuels and other human activities are currently adding more than 36 billion metric tons of CO<sub>2</sub> to the atmosphere each year<sup>3</sup>, producing an unprecedented build-up of this important greenhouse-forcing agent. Each year, terrestrial ecosystems sequester on average about a quarter of fossil fuel emissions and help mitigate global warming<sup>1–5</sup>. However, the nature, geographic distribution of land carbon sinks, and how their efficiencies change from year to year are not adequately understood, precluding an accurate prediction of their responses to future climate change and subsequent influences on climate through carbon cycle-climate feedbacks<sup>6,7</sup>. Recent evidence suggests that global semi-arid ecosystems provide an important contribution to the global land carbon sink and can dominate inter-annual variability and the trend of global terrestrial carbon cycle<sup>8,9</sup>.

Previous studies of the semi-arid carbon sink primarily relied on model outputs<sup>8,9</sup>. The results can be subject to uncertainties in input variables such as the assimilation of datasets that are sparse in many regions of the world, and may be further confounded by model assumptions, as suggested by a previous study finding that models can

<sup>1</sup>Climate Change Cluster, University of Technology Sydney, Broadway, New South Wales, 2007, Australia. <sup>2</sup>School of Life Sciences, University of Technology Sydney, Broadway, New South Wales, 2007, Australia. <sup>3</sup>Laboratoire des Sciences du Climat et de l'Environnement, CEA/CNRS/UVSQ, Gif-sur-Yvette, France. <sup>4</sup>NASA Goddard Space Flight Centre, Laboratory for Atmospheric Chemistry and Dynamics, Greenbelt, Maryland, 20771, United States. <sup>5</sup>Institute on Ecosystems and Department of Ecology, Montana State University, Bozeman, Montana, 59717, United States. <sup>6</sup>Jiangsu Provincial Key Laboratory of Geographic Information Science and Technology, International Institute for Earth System Sciences, Nanjing University, Nanjing, Jiangsu, 210023, China. <sup>7</sup>Jiangsu Center for Collaborative Innovation in Geographical Information Resource Development and Application, Nanjing, Jiangsu, 210023, China. <sup>8</sup>Helmholtz Centre Potsdam, GFZ German Research Centre for Geosciences, Potsdam, 14473, Germany. <sup>9</sup>Environment Institute, Ecology and Environment Science, University of Adelaide, South Australia, 5005, Australia. <sup>10</sup>USDA Agricultural Research Service, Southwest Watershed Research Centre, Tucson, Arizona, 85719, United States. Correspondence and requests for materials should be addressed to X.M. (email: xuanlong.ma@uts.edu.au)

differ substantially in predicting inter-annual variability of the terrestrial carbon cycle<sup>10,11</sup>. More importantly, these studies do not fully utilise ground measurements of carbon fluxes (e.g., from eddy-covariance flux towers). An observation-based study of the spatial attribution and temporal evolution of extreme wet-year driven carbon sinks over semi-arid regions has yet to be conducted to date.

Amplification of the hydrological cycle as a consequence of global warming is predicted to increase the frequency and severity of drought in the future<sup>12,13</sup>. These extreme drought events, if coupled with warmer temperatures, are expected to profoundly affect ecosystem function and structure, further exerting major impacts on the global carbon cycle and feedbacks to alter the rate of climate change<sup>13–20</sup>. Globally, a reduction in terrestrial primary productivity from 2000 to 2009 has been recorded primarily due to drought impact, which weakened the terrestrial carbon sink<sup>17</sup>. Regionally, the 2003 European warm-drought caused broad-scale declines in ecosystem productivity, led to a reverse of 4 years of carbon uptake<sup>21</sup>. The 2000–2004 drought reduced regional carbon uptake over western North America substantially<sup>22</sup>, and also caused large-scale vegetation die-off<sup>23–25</sup>, further releasing carbon stocks from biomass back to the atmosphere.

Global semi-arid ecosystems are mostly dominated by grasslands, shrublands, and savannas<sup>26–28</sup>. A combination of high biomass turnover rates and their presence in water-limited environments renders semi-arid ecosystems particularly sensitive to drought and wet events<sup>28–32</sup>. A recent study using flux tower measurements over semi-arid grasslands in southwest United States identified a precipitation threshold that a semi-arid system could switch from a net sink or a net source of carbon from year to year<sup>32</sup>. Meanwhile, a common temporal and spatial sensitivity of gross CO<sub>2</sub> uptake to water-availability over a broad diversity of semi-arid ecosystems in North America has also been reported<sup>33</sup>, indicating that fast ecophysiological responses are useful for predicting semi-arid carbon sink/source dynamics under future climatic water availability<sup>34</sup>. Global semi-arid ecosystems are currently threatened by increasing aridity and enhanced warming<sup>35,36</sup>, posing concerns on their sustainable ability to absorb carbon, maintain biodiversity, and support human livelihood. A better knowledge of the intrinsic link between hydroclimatic variations and carbon sink-source dynamics over global semi-arid regions, especially those within the Southern Hemisphere which have dominated the recent global land carbon sink anomaly<sup>8,9</sup>, is thus urgently needed. To-date, questions such as which ecosystems contributed most to the 2011 land carbon sink anomaly and how they respond when subsequently subjected to drought, remain largely unanswered. Carbon sink allocation into labile or more stable carbon reservoirs and the factors that govern source-sink sensitivity in semi-arid regions must be understood for prediction of long-term global carbon cycle-climate feedbacks.

Here, we assess the spatial allocation and temporal evolution of the land carbon sink over Australia in response to early 21<sup>st</sup>-century hydroclimatic variations. Australia, the driest inhabited continent in the world, is dominated by savannas, grasslands, and shrublands (Supplementary Fig. S1). We focus on Australia not only because of its recent impact on the global carbon cycle<sup>8,9</sup>, but also because it experiences the largest climate variability among the continents (Supplementary Fig. S2), thus it is of interest to know how ecosystems behave under such extreme climate variability. Specifically, we want to determine: (1) the detailed spatial allocation of the large net CO<sub>2</sub> uptake and variations in intrinsic efficiency of using rainfall for taking up carbon during abnormally wet periods; (2) the persistence of the large semi-arid net CO<sub>2</sub> uptake during throughout following dry period; and (3) the recurrence of Australia's large net CO<sub>2</sub> uptake in other wet years.

To answer these questions, we employed a multiple observation-based, interdisciplinary approach. To provide a “top-down” atmospheric view of the carbon dynamics, we used inverted net ecosystem carbon production (NEP) derived from satellite retrievals of CO<sub>2</sub> concentration from Japanese Greenhouse Gases Observing Satellite (GOSAT). We also used remote sensing of vegetation photosynthetic activity, including enhanced vegetation index (EVI) from the Moderate Resolution Imaging Spectroradiometer (MODIS) onboard NASA's Terra satellite and solar-induced chlorophyll fluorescence (SIF) from the Global Ozone Monitoring Experiment-2 (GOME-2) sensor onboard EUMETSAT's MetOp-A/B satellites. The EVI and SIF were used in a complementary manner, as SIF is emission-based and directly measures photosynthetic activity, while MODIS EVI is at a higher spatial resolution and enables the direct comparison with *in-situ* micrometeorological flux tower measurements. To characterize the hydroclimatic variations, we used the total water storage change (TWSC) from NASA's Gravity Recovery and Climate Experiment (GRACE) satellites and standardized precipitation-evapotranspiration drought index (SPEI) computed from long-term ground meteorological datasets. For SPEI, we used data computed at 6-month time scale considering the fact that vegetation across Australia primarily respond to drought at time-scales around 6-months or less. Lastly, as the most direct measure of ecosystem-atmosphere carbon exchange, we used NEP measured by *in-situ* eddy-covariance flux towers from two semi-arid ecosystems in Australia. Furthermore, to infer the contribution from fire emission to the semi-arid carbon-source dynamics, we employed the fire emission data from the fourth generation global fire emission database (GFED4.1s). A combination of multiple observation-based approaches will provide us the most direct and convergent evidence of the detailed spatial attribution, propensity, and the fate of the semi-arid carbon sink.

For our analyses, to accommodate the seasonal rainfall distribution over Australia, we used a ‘hydrological year’ instead of using a calendar year. The hydrological year is defined as from September to next August based on mean monthly rainfall climatology, such that precipitation falling within a hydrological year was mainly used within that year for vegetation productivity. In following text, a hydrological year such as 2010–11 represents a 12-months period from September-2010 to August-2011.

## Results and Discussion

Early 21<sup>st</sup>-century hydroclimatic variations spanning Australia were characterised by below average precipitation coupled with anomalously high temperature (Fig. 1a). Annual precipitation was below or near the historical average (1970–2013), while annual average temperature was above or near the historical average throughout nearly the entire 2001–02 to 2008–09 (Fig. 1a). This warm-dry period was enclosed by two wet periods, 2000–01 and 2010–11, with another wet period occurring in 2005–06 (Fig. 1a). Australia's terrestrial ecosystems were

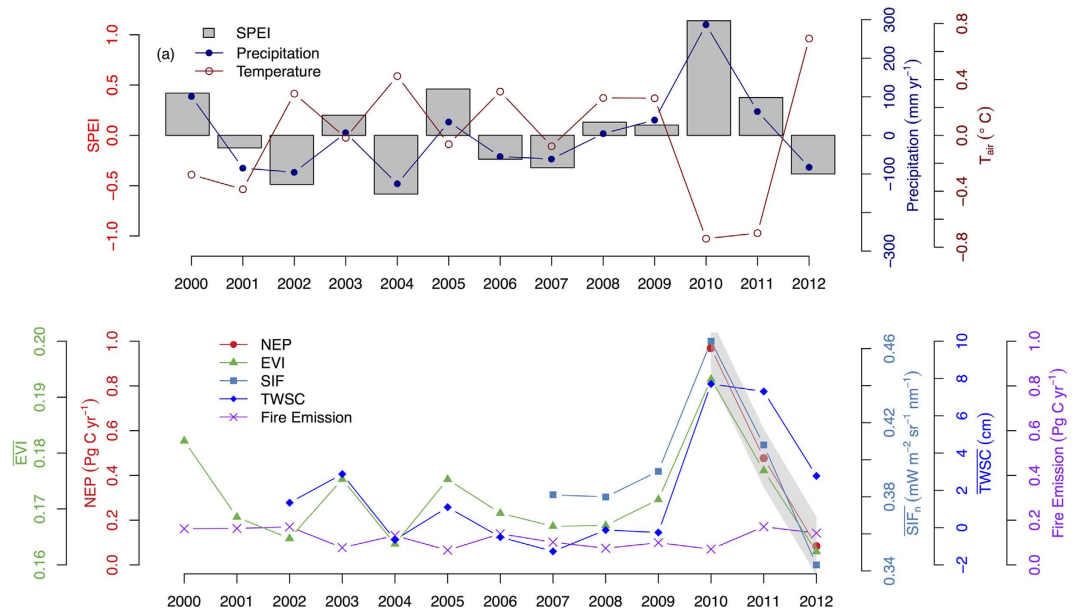


**Figure 1. Inter-annual variation in climate, carbon flux and terrestrial primary productivity of Australia from 2000–01 to 2012–13.** On the x-axis, 2000 represents the hydrological year starting from September–2000 to August–2011, and so on. **(a)** Variation in continental average annual Standardized Precipitation–Evapotranspiration drought Index (SPEI), anomaly of annual precipitation (mm yr<sup>-1</sup>), anomaly of annual mean daily temperature ( $T_{\text{air}}$ , °C) over Australia from 2000–01 to 2012–13. Anomalies of precipitation and temperature were computed with reference to the 1970–2013 base period. Positive SPEI indicates wetter than the historical median; negative values, drier than median; **(b)** Variation in continental summation of Net Ecosystem Production (NEP) (Pg C yr<sup>-1</sup>), continental average of annual integrated Enhanced Vegetation Index (EVI), continental average of Solar-Induced chlorophyll Fluorescence ( $\text{SIF}_n$ , PAR normalized SIF, mW m<sup>-2</sup> sr<sup>-1</sup> nm<sup>-1</sup>), continental average of Total Water Storage Change (TWSC, cm), and continental total fire carbon emission (Pg C yr<sup>-1</sup>). NEP is derived from GOSAT atmospheric inversion modeling. The gray shaded area represents the Bayesian uncertainty range of inverted NEP ( $\pm 1\sigma$ ).

strong carbon sinks in 2010–11 hydrological year ( $\sim 0.97$  Pg C yr<sup>-1</sup>) (Fig. 1b; Supplementary Table S1). This strong land carbon sink is corroborated by independent observations from MODIS EVI and GOME-2 SIF, both showing a much enhanced photosynthetic activity during the 2000–01, and 2010–11 wet episodes (Fig. 1b; Supplementary Table S1). The magnitude of the 2010–11 enhanced land carbon sink as derived from GOSAT inversion in this study, if reported based on calendar year, was 0.77 Pg in 2011, which is very similar with 0.79 Pg C reported by Poulter *et al.*<sup>8</sup> or 0.86 Pg C from another recent study<sup>37</sup>.

Consistent with the results from recent hydrological studies<sup>38,39</sup>, the large land carbon sink anomaly in 2010–11 corresponds with a large surplus of water storage (soil moisture + ground water) as indicated by GRACE TWSC (Fig. 1b). A sharp decline in both precipitation and GRACE TWSC after 2011, resulting in a dramatic reduction in NEP, EVI, and SIF from 2011 to 2013 and demonstrating the systematic link between semi-arid carbon sink-source dynamics and hydroclimatic variations (Fig. 1b). This is consistent with a recent study using Australian land surface model, constrained by multiple observational data sources<sup>40</sup>, which also reported a similar sharp decline in continental NEP after the 2010–11 wet period<sup>41</sup>.

Meanwhile, CO<sub>2</sub> emissions from fire burning were also enhanced following the 2010–11 productive wet period (Fig. 1b). The total fire emission over Australia, as estimated by GFED4.1s, was 0.07 Pg C in 2010–11,  $\sim 42\%$  below 2000–2013 average (Fig. 1b). The fire emission was boosted in 2011–12 (0.17 Pg C), one year followed the land carbon sink year, and was slightly reduced to 0.14 Pg C in 2012–13 (Fig. 1b; Supplementary Table S1). The total fire emission over Australia throughout the 2010–11 to 2012–13 period was 0.38 Pg C, about 25% of the size of total net carbon uptake (1.53 Pg C) over this period (Fig. 1b; Supplementary Table S1). This demonstrates the importance of fire emission as an important loss pathway over semi-arid ecosystems.

As a result of the combined effects from drought-induced reduction of photosynthetic activity and enhanced fire emissions, the percentage contribution of Australian terrestrial ecosystems to the global land carbon sink, as inferred from atmospheric inversion data, declined substantially from  $\sim 25\%$  in 2010–11 to  $\sim 13\%$  in 2011–12, and further reduced to  $\sim 2\%$  in 2012–13. These observation-based results demonstrate that the rapid reversals of semi-arid carbon sink anomalies are important contributors to the inter-annual variability of the global terrestrial carbon cycle, as was shown through previous studies<sup>8,9,42</sup>.

Meanwhile, our results also indicate the potential ecological resilience of Australia's dryland ecosystems to altered hydroclimatic conditions, as they were able to sequester large amounts of carbon after protracted dry periods (Fig. 1). The resilience of Australian semi-arid ecosystems to drought may be attributed to the fact that these ecosystems are dominated by perennial, drought tolerant species such as *Acacia spp.* (mulga) and *Triodia spp.* (spinifex), each covers ca. 30–35% of Australian semi-arid land area<sup>43</sup>. These species can maintain foliage

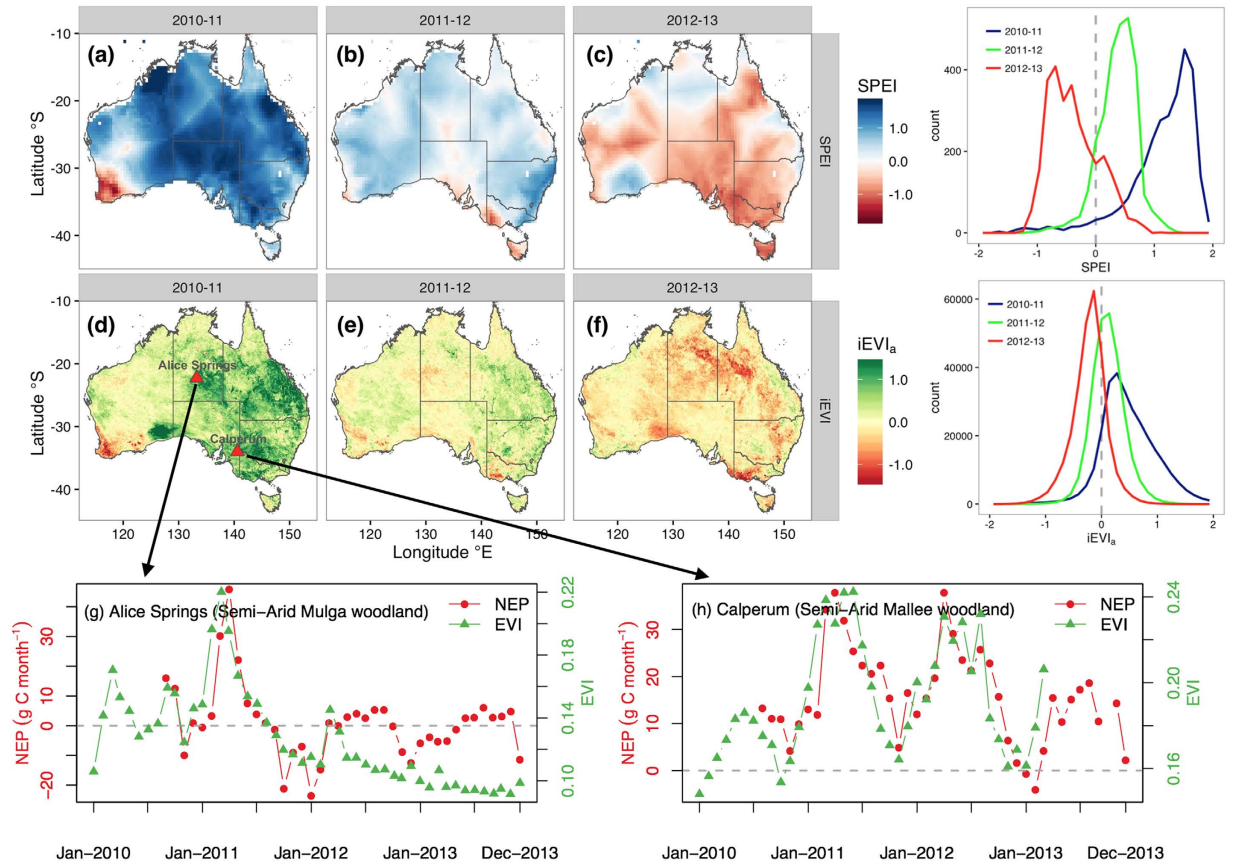


**Figure 2. Biogeographic pattern of hydroclimatic condition and terrestrial primary productivity across Australia from 2010–11 to 2012–13.** (a–c) maps of annual average SPEI; (d–f) maps of annual terrestrial primary productivity anomaly (surrogated by anomaly of annual integrated EVI, or  $iEVI_a$ ); (g–h) MODIS EVI alongside with *in-situ* eddy-covariance tower measured NEP at Alice Springs (semi-arid Mulga woodland) and Calperum (semi-arid Mallee woodland) from Jan-2010 to Dec-2013. Right panels show frequency distribution of SPEI and  $iEVI_n$  for 2010–11 (blue), 2011–12 (green), and 2012–13 (red) using data from the all of Australia respectively. Maps were drawn using R version 3.1.2 (<http://www.r-project.org/>).

and minimal metabolic activity during the dry season or drought periods, largely attributed to their highly drought-adapted hydraulic architecture and their ability to tap deep soil water reserves with their lengthy root systems. Meanwhile, drought-adapted biota in these ecosystems also resulted in asymmetric response of Australia's dryland ecosystems to rainfall, in which these ecosystems responded more strongly to wet than to dry period<sup>44</sup>. As a result of above potential mechanisms, Australian semi-arid ecosystems were able to contribute to 2011 global land carbon sink anomaly significantly after the protracted early 21<sup>st</sup>-century warm-dry period, further demonstrating the resilient nature of Australian semi-arid carbon sink (Fig. 1). Future studies are needed to look at the historical data in order to better understand the ecological resilience of Australia's dryland ecosystems in response to multiple drought and wet periods.

Carbon exchange over Australia is substantially affected by large-scale contrasting drought and wet conditions (Fig. 2). There was a transition from anomalously wet conditions in 2010–11 (SPEI = 1.14) to anomalously dry condition in 2012–13 (SPEI = -0.38), especially over eastern Australia (Fig. 2a–c; Supplementary Fig. S3). At the same time, the positive anomaly of MODIS EVI in 2011 switched to a negative anomaly in 2012, and by 2013, most areas of Australia exhibited a strong negative MODIS EVI anomaly, suggesting a significant reduction in terrestrial primary productivity and associated weakening of the strength of the carbon sink under drought (Fig. 2d–f; Supplementary Fig. S3).

As the most direct measurement of carbon exchange between an ecosystem and the atmosphere, *in-situ* eddy-covariance (EC) flux tower measurements of NEP at two semi-arid ecosystems were used as ground-truth to verify the patterns in the temporal evolution of carbon fluxes as estimated from the “top-down” methods (Fig. 2g,h). At Alice Springs, the ecosystem was a net sink of carbon in 2011, and rapidly switched to a weak carbon source in subsequent 2012 and 2013 drought years<sup>43</sup> (Fig. 2g). At Calperum, each year from 2011 to 2013 was a net sink of carbon, although the strength was weakened substantially in 2013 due to drought (Fig. 2h). Most importantly, we found strong agreement between *in-situ* EC flux tower measured NEP and MODIS EVI (Fig. 2g,h), suggesting that temporal variations in carbon fluxes at these semi-arid ecosystems were primarily driven by photosynthetic activity during the carbon sink period. This finding also supports the use of satellite measures of photosynthetic activity (MODIS EVI and GOME-2 SIF) for depicting the spatial allocation of the

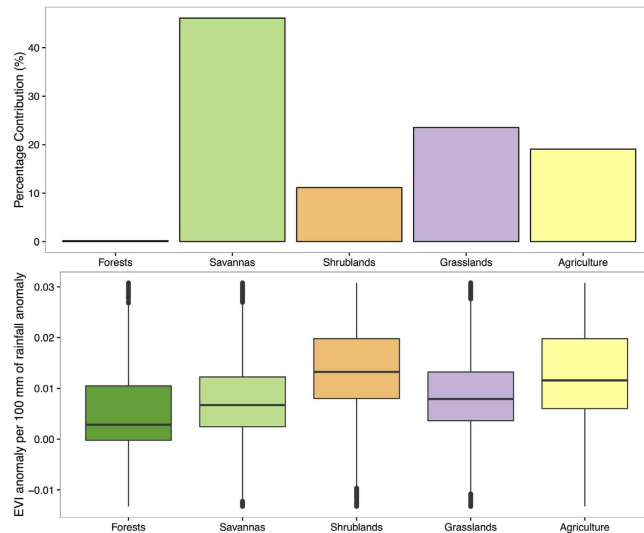


**Figure 3. Partitioning of Australia's terrestrial primary productivity into contributions from major biomes during the 2010–11 carbon sink period.** (a) Percentage contribution of each biome to Australian 2010–11 productivity anomaly (as indicated by anomaly of EVI). The percent contribution was calculated using MODIS EVI. For each measure, the anomaly of EVI in 2010–11 hydrological year was calculated and then partitioned spatially into different biome type; (b) box-plot of EVI anomaly in 2010–11 per 100 mm of rainfall anomaly in 2010–11 generated using all pixels within each biome. This is equivalent to the normalisation of EVI anomaly for each biome by its total area and then further by rainfall anomaly. Thus the ratio is a measure of intrinsic efficiency of an ecosystem in using rainfall for taking up carbon. The upper and lower hinges of the box-plot correspond to the first and third quartiles (the 25th and 75th percentiles) of the data, while the upper and lower whiskers correspond to the maximum and the minimum value of the data. The thick horizontal line within the box represents the median value of the data.

carbon sink over dryland ecosystems. Meanwhile, we also note the divergence between MODIS EVI and EC flux-tower NEP at Alice Springs during the carbon source period (2012–2013) (Fig. 2g), suggesting that remote sensing measures of photosynthesis is less suitable for identifying the location of carbon emissions during the source period, while more useful for inferring the location of carbon reservoirs during the sink period. The discrepancy between EVI and NEP during the dry period is likely due to: 1) EVI is a measure of photosynthetic capacity, which is more related to net primary productivity (NPP, the difference between photosynthesis and autotrophic respiration); 2) NEP is a balance between photosynthesis and ecosystem respiration. When NEP is primarily driven by variations in photosynthesis, it is expected to see a good correlation between NEP and EVI, as we saw during the land carbon sink year (Fig. 2g). When ecosystem is under drought stress and thus NEP is primarily driven by variations in ecosystem respiration, there should be a divergence between EVI and NEP, as during the period following the land carbon sink year (Fig. 2g).

We have shown that the NEP of carbon is primarily driven by photosynthesis during the carbon sink period over Australia's dryland ecosystems (Fig. 2g,h). We thus inferred the spatial location of the strength of net CO<sub>2</sub> uptake by partitioning anomaly of MODIS EVI into Australia's major biomes during the 2010–11 carbon sink period (Fig. 3). Among major biomes, savannas and grasslands had the highest rates of primary productivity anomaly during the 2010–11 La Niña wet periods (Figs 2d and 3a; Supplementary Fig. S1, Table S2). In 2010–11, about 46% of the terrestrial primary productivity anomaly was attributed to savannas and 24% to grasslands (Figs 2d and 3a; Supplementary Fig. S1, Table S2), implying that these two biomes were potentially the biomes with the largest net CO<sub>2</sub> uptake in Australia during the carbon sink anomaly year, which is in line with another study based on model simulation<sup>45</sup>. The consistency between these independent studies increases the confidence of the spatial partition of the 2010–11 net CO<sub>2</sub> uptake into different biomes.

To further understand the variation in efficiency of using rainfall for taking up carbon during the 2010–11 carbon sink year, we calculated the ratio between MODIS EVI anomaly and rainfall anomaly for each pixel across Australia during the 2010–11 wet pulse. Our results showed that, despite the fact that savannas and grasslands are potentially the biomes with the largest net CO<sub>2</sub> uptake in 2010–11, shrublands, which are primarily located over central and southern Australia, have the highest efficiency in using rainfall anomaly for taking up carbon (Fig. 3b; Supplementary Fig. S4, Table S2). Our results indicated that mean rain-use-efficiency of shrublands is significantly higher ( $p < 0.0001$ , Student's *t*-Test) than that of grasslands, and also significantly higher ( $p < 0.0001$ ) than that of savannas. Meanwhile, our results also highlighted the large within-biome variation in efficiency of using rainfall for generating productivity anomaly, as indicated by the fact that coefficient of variation (standard deviation/mean) ranges from 60% (shrublands) to 240% (forests) (Supplementary Fig. S4, Table S2). The much larger response of vegetation productivity to very wet year over drier shrublands than wetter biomes such as savannas and forests is likely due to the pulse-response behaviour of the drought-adapted plants in these ecosystems<sup>44</sup>. Besides, we also noticed that for sparsely vegetated areas which have the largest positive asymmetric response

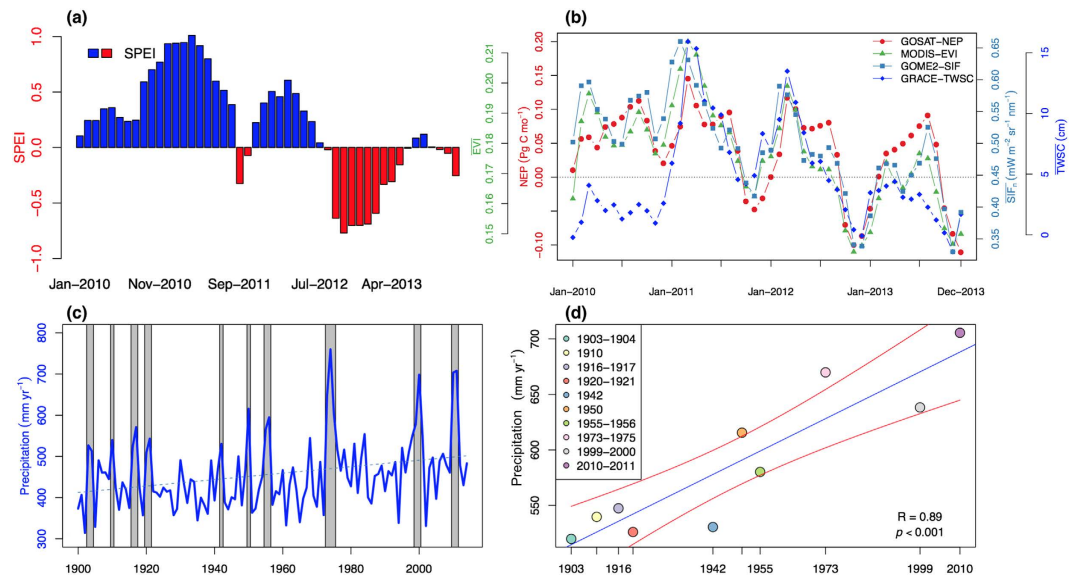


**Figure 4.** Reduction of net CO<sub>2</sub> uptake over Australia as determined by subsequent hydroclimatic conditions. (a) Monthly SPEI averaged across Australia from 2010 to 2013; (b) Variations of monthly NEP, EVI, SIF, and TWSC aggregated across Australia from 2010 to 2013; (c) time series of average annual precipitation across Australia from 1900 to 2013. Blue dashed line is the trend line, while grey vertical bars indicate each very wet period since 1900; (d) trend in precipitation amount during the very wet periods (e.g., 2010–11). Blue line is linear regression line and red lines indicate 95% confidence intervals. Before calculating the precipitation amount during the very wet periods, the precipitation time series has been linearly detrended.

of vegetation productivity to wet year<sup>44</sup>, our results showed that part of these sparsely vegetated ecosystems, primarily in Western Australia, did not exhibit a strong productivity response in 2010–11 (Supplementary Fig. S4). The lack of response of these ecosystems to 2010–11 wet year may be attributed to the fact that a persistent decline in GRACE terrestrial water storage (TWS) trend has been observed over Western Australia since 2002<sup>39</sup>. This drying trend as indicated by GRACE TWS imply that vegetation over these regions were stressed during the 2002–2009 period and may have lost resilience, thus unable to respond strongly to the 2010–11 wet year. Future studies, with the incorporation of more field observations, are needed to investigate the exact mechanisms that explain the lack of response of ecosystems over Western Australia to the wet period. These patterns of varying rain-use-efficiency, as derived from observational datasets, are informative and reflect the differences in ecosystem-level carbon-water relationship. Therefore, Earth system models may consider using these patterns as observational test. Specifically, models may test their capability of simulating the spatial nature of the response of terrestrial carbon uptake per unit change in rainfall amount during the extreme wet years, i.e., the sensitivity of terrestrial carbon uptake to precipitation anomaly.

We have shown that Australia's ecosystems are strong sinks of CO<sub>2</sub> during extreme wet periods. An important question that remains is to what extent the strength of the wet year-stimulated net CO<sub>2</sub> uptake is sustained through non-wet years? Throughout the entire 2010–11 wet period, Australia's ecosystems remained a large carbon sink, manifested by enhanced photosynthetic activity marked by high MODIS EVI and GOME-2 SIF values (Fig. 4a,b). This active state continued into the first half of 2012 at a much lower rate, owing to reduced water availability as indicated by both SPEI and GRACE TWSC (Fig. 4a,b; Supplementary Fig. S5). Dry conditions prevailed from the late half of 2012 to 2013, resulting in a significant reduction of the net CO<sub>2</sub> uptake from a strong net sink (−0.77 Pg C in 2010) to a weak sink (−0.12 Pg C in 2013), a 85% reduction in the strength of net CO<sub>2</sub> uptake (Fig. 4a,b; Supplementary Fig. S5). Our multiple observation-based datasets thus demonstrated the fact that the large semi-arid net CO<sub>2</sub> uptake originated from extreme La Niña wet period to be very short-lived and a transitory event, in which drought occurrence can rapidly reduce the magnitude of carbon uptake (Fig. 4a,b; Supplementary Fig. S5).

Australia is situated in a region of extreme climate variability, creating several-fold larger fluctuations in precipitation and terrestrial primary productivity than encountered in all other continents (Supplementary Fig. S2). Exceptionally large vegetation productivity was recorded over Australia during both of the recent two La Niña-induced very wet periods (2000–01 and 2010–11) (Fig. 1b), thus demonstrating that the large land carbon sink of Australia reported in 2010–11 was not an isolated and unique event, but rather a potentially episodic occurrence under strong wet phases. This is also reflected by the enhanced fire emissions throughout both the 2000–01 to 2002–03 and 2010–11 to 2012–13 periods (Fig. 1b). Precipitation and hence soil moisture availability are the primary drivers of semi-arid ecosystems carbon dynamics<sup>44</sup>; we therefore expect that the exceptionally large land carbon sink, coupled to very wet phases, will be observed again in the future.

An intriguing and important question is whether the magnitude of Australia's next carbon sink in a future wet episode will exhibit a similar strength as in 2010–11 or whether it will become stronger or weaker? The historical climatological record for Australia reveals that the precipitation amounts during wet years, such as 2000–01

and 2010–11, have increased significantly since 1900 (increasing by 11.66 mm per year,  $p < 0.05$ ) (Fig. 3c–d; Supplementary Fig. S6). Meanwhile, an overall wetting trend has resulted in the expansion of vegetation cover over Australia since 1981<sup>8,46</sup> (Fig. 4c; Supplementary Fig. S7). Recent study has found that dryland ecosystems in Australia tend to respond more strongly to wet period than drought, i.e., positive asymmetric type of responses, attributable to the pulse-response behaviour of these drought-adapted plants<sup>44</sup>. These findings together suggested that the magnitudes of the Australian semi-arid sink associated with wet-extremes will increase in coming decades. The consequence of this trend will have important implications for global carbon cycling, as shown during the 2011 global land carbon sink anomaly period<sup>8,9</sup>.

In summary, multiple independent lines of evidence create a compelling argument that extreme wet year driven, semi-arid land carbon sink events are transient and dissipate rapidly under ensuing drought. The efficiencies of these semi-arid carbon sinks are highly sensitive to hydroclimatic variations and are particularly vulnerable to drought. The spatial attribution of the land carbon sink to tropical savannas and grasslands refines previous attributions to semi-arid ecosystems<sup>7,8</sup>. The finding of large variations in rainfall use efficiency among biomes for generating productivity anomaly in 2010–11 provides insight into the intrinsic effectiveness for taking up carbon. The two large carbon sink events, in 2000–01 and 2010–11, were coupled with La Niña-induced wet pulses, and demonstrated an episodic nature of Australia's land carbon sink. Given a continuation of the increasing trend in extreme wet-year precipitation amounts since 1900 over Australia, we hereby suggest that the large land carbon sink will be observed again with greater magnitude in the future. We conclude that by contributing more positively to the global carbon balance with greater net CO<sub>2</sub> uptake during the forthcoming more intensive very wet years, Australia's ecosystems will play a more significant role in the global carbon cycle in coming decades. This study also demonstrated the great potential of integrating satellite and surface observations to provide a big, unifying picture of terrestrial carbon sink-source dynamics over a continental scale. The use of multiple observational data sources (e.g., GOSAT atmospheric CO<sub>2</sub> sampling, GOME-2 SIF, and GRACE TWSC) increases the robustness of land carbon sink-source analyses that will essentially lead to an improved understanding of the hydroclimatic drivers and pulse response behaviour of carbon fluxes over dryland ecosystems. The rapid dissipation of large semi-arid net CO<sub>2</sub> uptake under drought as revealed by this study presents important observational tests for Earth System models to accurately depict terrestrial carbon dynamics under intensified hydrological extremes.

## Methods

We use multiple observation-based data sources to diagnose the geographic distribution and temporal evolution of Australia's land carbon sinks in extremely wet years. Continental-wide biospheric CO<sub>2</sub> fluxes were inverted using retrievals of atmospheric CO<sub>2</sub> from Japanese Greenhouse gases Observing SATellite (GOSAT), with the Bayesian uncertainty statistics of the estimated fluxes were defined by a posterior error covariance matrix (see Supplementary information: Atmospheric inversion of biospheric carbon fluxes). Vegetation photosynthetic activity was indicated by two satellite measures: (1) Enhanced Vegetation Index (EVI), which is a composite measure of leaf area, chlorophyll content, and canopy architecture, derived from Moderate Resolution Imaging Spectroradiometer (MODIS) on-board NASA's Terra satellite (MOD13C1, Collection 5); (2) Solar-Induced chlorophyll-Fluorescence (SIF), which is emitted by the photosystem II of the chlorophyll molecules of assimilating leaves, derived from the Global Ozone Monitoring Experiment-2 (GOME-2) instrument on-board EUMETSAT's MetOp-A/B satellites (version 26, level-3) (see Supplementary information: Satellite measured vegetation photosynthetic capacity). To determine drought severity, we use the Standardised Precipitation-Evapotranspiration Index (SPEI), which is a multi-scalar drought index that takes into account both precipitation and temperature (see Supplementary information: Standardised Precipitation-Evapotranspiration drought Index). Total water storage change (TWSC) derived from NASA's Gravity Recovery and Climate Experiment (GRACE) observations was used as an integrative measure of water storage change over continental scale (see Supplementary information: GRACE Terrestrial Total Water Storage Change). We use gridded rain gauge and temperature datasets provided by the National Climate Centre, Australian Bureau of Meteorology (see Supplementary information: Gridded meteorological datasets). Micrometeorological flux tower measured net ecosystem production (NEP) data (Level 3) is provided by OzFLUX network (see Supplementary information: *In-situ* measurements of NEP). To infer the contribution of fire emissions to the sink-source dynamics and further refine our understanding of carbon loss pathway over semi-arid ecosystems, we used fire emission data from the fourth-generation global fire emissions database (GFED4.1s) (see Supplementary information: Global Fire Emissions Database). Major vegetation group map provided by Australian National Vegetation Information System (NVIS, v4.1) was used to derive the contribution of each biome type to continental carbon fluxes (see Supplementary information: Vegetation map). The 26 NVIS vegetation groups were grouped into five major biomes: forest, savanna, shrubland, grassland, and agriculture. The savanna biome, a tree-shrub-grass multi-strata system, includes all open forests, woodlands, as well as parts of shrublands, with both *Eucalyptus*, *Acacia* or other trees as the dominant canopy species. The grassland biome includes hummock grassland, tussock grassland, and other grassland types.

## References

- Keeling, C. D., Chin, J. F. S. & Whorf, T. P. Increased activity of northern vegetation inferred from atmospheric CO<sub>2</sub> measurements. *Nature* **382**, 146–149 (1996).
- Dlugokencky, E. & Tans, P. ESRL Global Monitoring Division – Global Greenhouse Gas Reference Network. [www.esrl.noaa.gov/gmd/ccgg/trends/](http://www.esrl.noaa.gov/gmd/ccgg/trends/) (Date of access: 13/09/2016) (2015).
- Le Quéré, C. *et al.* The global carbon budget 1959–2011. *Earth Syst Sci Data* **5**, 165–185 (2013).
- Raupach, M. R. *et al.* Global and regional drivers of accelerating CO<sub>2</sub> emissions. *Proc Natl Acad Sci USA* **104**, 10288–10293 (2007).
- Pan, Y. *et al.* A Large and Persistent Carbon Sink in the World's Forests. *Science*, **333**, 988–993 (2011).
- Friedlingstein, P. *et al.* Climate-carbon cycle feedback analysis: results from the C4MIP model intercomparison. *J Climate* **19**, 3337–3353 (2006).

7. Canadell, J. G. *et al.* Contributions to accelerating atmospheric CO<sub>2</sub> growth from economic activity, carbon intensity, and efficiency of natural sinks. *Proc Natl Acad Sci USA* **104**, 18866–18870 (2007).
8. Poulter, B. *et al.* Contribution of semi-arid ecosystems to interannual variability of the global carbon cycle. *Nature* **509**, 600–603 (2014).
9. Ahlström, A. *et al.* The dominant role of semi-arid ecosystems in the trend and variability of the land CO<sub>2</sub> sink. *Science* **348**, 895–899 (2015).
10. Keenan, T. F. *et al.* Terrestrial biosphere model performance for inter-annual variability of land-atmosphere CO<sub>2</sub> exchange. *Glob Change Biol.* **18**, 1971–1987 (2012).
11. Yi, C. *et al.* Climate control of terrestrial carbon exchange across biomes and continents. *Environ Res Lett* **5**, 034007 (2010).
12. Prudhomme, C. *et al.* Hydrological droughts in the 21st century, hotspots and uncertainties from a global multimodel ensemble experiment. *Proc Natl Acad Sci USA* **111**, 3262–3267 (2014).
13. Yi, C., Pendall, E. & Ciais, P. Focus on extreme events and the carbon cycle. *Environ Res Lett* **10**, 070201 (2015).
14. Rammig, A. & Mahecha, M. D. Ecology: Ecosystem responses to climate extremes. *Nature* **527**, 315–316 (2016).
15. Ciais, P. *et al.* Europe-wide reduction in primary productivity caused by the heat and drought in 2003. *Nature* **437**, 529–533 (2005).
16. Zeng, N., Qian, H., Rödenbeck, C. & Heimann, M. Impact of 1998–2002 midlatitude drought and warming on terrestrial ecosystem and the global carbon cycle. *Geophys Res Lett* **32**, L22709 (2005).
17. Zhao, M. & Running, S. W. Drought-induced reduction in global terrestrial Net Primary Production from 2000 through 2009. *Science* **329**, 940–943 (2010).
18. Reichstein, M. *et al.* Climate extremes and the carbon cycle. *Nature* **500**, 287–295 (2013).
19. Anderegg, W. R. L. *et al.* Pervasive drought legacies in forest ecosystems and their implications for carbon cycle models. *Science*, **349**, 528–532 (2015).
20. Forkel, M. *et al.* Enhanced seasonal CO<sub>2</sub> exchange caused by amplified plant productivity in northern ecosystems. *Science*, **351**, 696–699 (2016).
21. Reichstein, M. *et al.* Reduction of ecosystem productivity and respiration during the European summer 2003 climate anomaly: a joint flux tower, remote sensing and modelling analysis. *Glob Change Biol* **13**, 634–651 (2007).
22. Schwalm, C. R. *et al.* Reduction in carbon uptake during turn of the century drought in western North America. *Nat Geosci* **5**, 551–556 (2012).
23. Breshears, D. D. *et al.* Regional vegetation die-off in response to global-change-type drought. *Proc Natl Acad Sci USA* **102**, 15144–15148 (2005).
24. Fensham, R. J. *et al.* Drought-induced tree death in savanna. *Glob Change Biol* **15**, 380–387 (2009).
25. Huang, K. *et al.* Tipping point of a conifer forest ecosystem under severe drought. *Environ Res Lett* **10**, 024011 (2015).
26. Sage, R. F., Christin, P. A. & Edwards, E. J. The C<sub>4</sub> plant lineages of planet Earth. *J Exp Bot* **62**, 3155–3169 (2011).
27. Morgan, J. A. *et al.* C<sub>4</sub> grasses prosper as carbon dioxide eliminates desiccation in warmed semi-arid grassland. *Science* **476**, 202–205 (2011).
28. Cherwin, K. & Knapp, A. Unexpected patterns of sensitivity to drought in three semi-arid grasslands. *Oecologia* **169**, 845–852 (2012).
29. Ponce-Campos, G. E. *et al.* Ecosystem resilience despite large-scale altered hydroclimatic conditions. *Nature* **494**, 349–352 (2013).
30. Moran, M. S. *et al.* Functional response of U.S. grasslands to the early 21st-century drought. *Ecology* **95**, 2121–2133 (2014).
31. Ma, X., Huete, A., Moran, M. S., Ponce-Campos, G. & Eamus, D. Abrupt shifts in phenology and vegetation productivity under climate extremes. *J Geophys Res G* **120**, 2036–2052 (2015).
32. Scott, R. L., Biederman, J. A., Hamerlynck, E. P. & Barron-Gafford, G. A. The carbon balance pivot point of southwestern U.S. semiarid ecosystems: Insights from the 21st century drought. *J Geophys Res G* **120**, 2612–2624 (2015).
33. Yi, C. *et al.* Climate extremes and grassland potential productivity. *Environ Res Lett* **7**, 035703 (2012).
34. Biederman, J. A. *et al.* Terrestrial carbon balance in a drier world: the effects of water availability in southwestern North America. *Glob Change Biol* **22**, 1867–1879 (2016).
35. Yi, C., Wei, S. & Hendrey, G. Warming climate extends dryness-controlled areas of terrestrial carbon sequestration. *Sci Rep* **4**, 5472 (2014).
36. Huang, J., Yu, H., Guan, X., Wang, G. & Guo, R. Accelerated dryland expansion under climate change. *Nat Clim Change* **6**, 166–171 (2016).
37. Detmers, R. G. *et al.* Anomalous carbon uptake in Australia as seen by GOSAT. *Geophys Res Lett* **42**, 8177–8184 (2015).
38. Boening, C. *et al.* The 2011 La Niña: So strong, the oceans fell. *Geophys Res Lett* **39**, L19602 (2012).
39. Xie, Z. *et al.* Spatial partitioning and temporal evolution of Australia's total water storage under extreme hydroclimatic impacts. *Remote Sens Environ.* **183**, 43–52 (2016).
40. Haverd, V. *et al.* The Australian terrestrial carbon budget. *Biogeosci* **10**, 851–869 (2013).
41. Haverd, V., Smith, B. & Trudinger, C. Dryland vegetation response to wet episode, not inherent shift in sensitivity to rainfall, behind Australia's role in 2011 global carbon sink anomaly. *Global Change Biol.* **22**, 2315–2316 (2016).
42. Huang, L. *et al.* Drought dominates the interannual variability in global terrestrial net primary production by controlling semi-arid ecosystems. *Sci Rep* **6**, 1–6 (2016).
43. Cleverly, J. *et al.* Productivity and evapotranspiration of two contrasting semiarid ecosystems following the 2011 global carbon land sink anomaly. *Agri For Met.* **220**, 151–159 (2016).
44. Haverd, V., Ahlström, A., Smith, B. & Canadell, J. G. Carbon cycle responses of semi-arid ecosystems to positive asymmetry in rainfall. *Glob Change Biol* (2016).
45. Haverd, V., Smith, B. & Trudinger, C. Process contributions of Australian ecosystems to interannual variations in the carbon cycle. *Environ Res Lett* **11**, 054013 (2016).
46. Donohue, R. J. *et al.* Climate-related trends in Australian vegetation cover as inferred from satellite observations, 1981–2006. *Glob Change Biol* **15**, 1025–1039 (2009).

## Acknowledgements

This work was funded by an Australian Research Council - Discovery Project “Impact of extreme hydro-meteorological conditions on ecosystem functioning and productivity patterns across Australia” (ARC-DP140102698, CI Huete). The first author also acknowledges the support from an Early Career Research Grant (ECRG) from University of Technology Sydney “Fingerprinting Australian ecosystem threats from climate change and biodiversity loss” (PRO16-1358, CI Ma). We would like to thank the opening of flux tower data for public access by the Australian Terrestrial Ecosystem Research Network (TERN, [www.tern.org.au](http://www.tern.org.au)) – OzFlux facility ([www.ozflux.org.au](http://www.ozflux.org.au)), as well as the availability of multiple processed satellite products by TERN's AusCover remote sensing facility ([www.auscover.org.au](http://www.auscover.org.au)). The ACOS GOSAT data can be obtained from <http://co2.jpl.nasa.gov>. They were produced by the ACOS/OCO-2 project at the Jet Propulsion Laboratory, California Institute of Technology, using GOSAT observed spectral radiances made available by the GOSAT project.

### Author Contributions

X.M. and A.H. conceived the idea and designed the study. X.M. conducted the analyses. X.M., A.H., J.C., and D.E. drafted the manuscript. F.C., J.C., D.E., J.J., W.M., Z.X. contributed data to the analysis. B.P., Y.Z., L.G., and G.P.C. contributed to the interpretations of the results and manuscript writing. All authors contributed to the manuscript revision.

### Additional Information

**Supplementary information** accompanies this paper at <http://www.nature.com/srep>

**Competing financial interests:** The authors declare no competing financial interests.

**How to cite this article:** Ma, X. *et al.* Drought rapidly diminishes the large net CO<sub>2</sub> uptake in 2011 over semi-arid Australia. *Sci. Rep.* **6**, 37747; doi: 10.1038/srep37747 (2016).

**Publisher's note:** Springer Nature remains neutral with regard to jurisdictional claims in published maps and institutional affiliations.



This work is licensed under a Creative Commons Attribution 4.0 International License. The images or other third party material in this article are included in the article's Creative Commons license, unless indicated otherwise in the credit line; if the material is not included under the Creative Commons license, users will need to obtain permission from the license holder to reproduce the material. To view a copy of this license, visit <http://creativecommons.org/licenses/by/4.0/>

© The Author(s) 2016

# Supplementary Information

## Drought rapidly diminishes the large net CO<sub>2</sub> uptake in 2011 over semi-arid Australia

Xuanlong Ma<sup>a,\*</sup>, Alfredo Huete<sup>a</sup>, James Cleverly<sup>b</sup>, Derek Eamus<sup>b</sup>, Frédéric Chevallier<sup>c</sup>,  
Joanna Joiner<sup>d</sup>, Benjamin Poulter<sup>e</sup>, Yongguang Zhang<sup>f,g</sup>, Luis Guanter<sup>h</sup>, Wayne Meyer<sup>i</sup>,  
Zunyi Xie<sup>a</sup>, and Guillermo Ponce-Campos<sup>j</sup>

<sup>a</sup> Climate Change Cluster, University of Technology Sydney, Broadway, New South Wales, 2007 Australia;

<sup>b</sup> School of Life Sciences, University of Technology Sydney, Broadway, New South Wales, 2007 Australia;

<sup>c</sup> Laboratoire des Sciences du Climat et de l'Environnement, CEA/CNRS/UVSQ, Gif-sur-Yvette, France;

<sup>d</sup> NASA Goddard Space Flight Centre, Laboratory for Atmospheric Chemistry and Dynamics, Greenbelt, Maryland, 20771 United States;

<sup>e</sup> Institute on Ecosystems and Department of Ecology, Montana State University, Bozeman, Montana, 59717 United States;

<sup>f</sup> Jiangsu Provincial Key Laboratory of Geographic Information Science and Technology, International Institute for Earth System Sciences, Nanjing University, Nanjing, Jiangsu, 210023 China;

<sup>g</sup> Jiangsu Center for Collaborative Innovation in Geographical Information Resource Development and Application, Nanjing, Jiangsu, 210023 China;

<sup>h</sup> Helmholtz Centre Potsdam, GFZ German Research Centre for Geosciences, Potsdam, 14473 Germany;

<sup>i</sup> Environment Institute, Ecology and Environment Science, University of Adelaide, South Australia, 5005 Australia;

27 <sup>j</sup> USDA Agricultural Research Service, Southwest Watershed Research Centre, Tucson,  
28 Arizona, 85719 United States

29 \* Author to whom correspondence should be addressed X.M. (email:  
30 xuanlong.ma@uts.edu.au).

31

32 **This supplementary information file contains:**

33 1. Supplementary materials and methods

34 *1.1. Atmospheric inversion of biospheric carbon fluxes*

35 *1.2. Satellite measured vegetation photosynthetic capacity*

36 *1.3. In-situ measurements of net ecosystem carbon exchange by eddy-covariance flux*  
37 *towers*

38 *1.4. Standardised Precipitation-Evapotranspiration drought Index*

39 *1.5. GRACE Terrestrial Total Water Storage Change*

40 *1.6. Gridded meteorological datasets*

41 *1.7. Global fire emissions database*

42 *1.8. Identifying precipitation pulses*

43 *1.9. Vegetation map*

44 2. Supplementary table and figures

45 3. Supplementary references

46

47 **1. Supplementary materials and methods**

48 ***1.1 Atmospheric inversion of biospheric carbon fluxes***

49 Atmospheric CO<sub>2</sub> inversions estimate surface carbon fluxes from an "atmospheric point of  
50 view" (i.e., "top-down"), using an atmospheric transport model by optimally fitting, in a  
51 statistical sense, the high-fidelity atmospheric measurements of CO<sub>2</sub> concentration sampled  
52 from a global network of more than 100 sites and prior information about the carbon fluxes<sup>1</sup>.

53 To improve the density of atmospheric CO<sub>2</sub> measurements, remote sensing techniques have  
54 been developed for retrieving column-averaged dry air CO<sub>2</sub> mole fractions ( $\chi$ CO<sub>2</sub>) from  
55 satellite radiance measurements<sup>2-3</sup>. The Thermal And Near-infrared Sensor for carbon  
56 Observation-Fourier transform spectrometer (TANSO-FTS) onboard the Japanese  
57 Greenhouse Gas Observing Satellite (GOSAT) is the first instrument that was designed to  
58 provide the accuracy, resolution, and coverage that are sufficient to characterize the  
59 variability of regional sources and sinks of CO<sub>2</sub> on seasonal and inter-annual time

60 scales<sup>4</sup>. The use of such data is still in its learning phase<sup>5</sup>, but Australia is a part of the globe  
61 where GOSAT inversion results appear to be robust<sup>6</sup>. In this study we use CO<sub>2</sub> surface fluxes  
62 inferred from NASA's Atmospheric CO<sub>2</sub> Observations from Space project retrievals, build  
63 3.5 (ACOS B3.5). The inversion scheme is the global one from the Monitoring Atmospheric  
64 Composition and Climate service (MACC, [www.copernicus-atmosphere.org](http://www.copernicus-atmosphere.org))<sup>7</sup>. The MACC  
65 inversion scheme is based on an LMDZ (Laboratoire de Météorologie Dynamique)  
66 atmospheric transport model<sup>8</sup>, while the prior fluxes are estimated using the ORCHIDEE  
67 (Organising Carbon and Hydrology In Dynamic Ecosystems) land surface model<sup>9</sup>, and fire  
68 emission is obtained from Global Fire Emissions Database (GFED) version 4.1<sup>10</sup>. Uncertainty  
69 of the inverted CO<sub>2</sub> surface fluxes is estimated using the Bayesian error statistics defined by a  
70 posterior error covariance matrix. This matrix has been computed from a stochastic ensemble  
71 of inversions that is consistent with the assigned prior error statistics and with the assigned  
72 observation error statistics<sup>11</sup>.

### 73 ***1.2 Satellite measured vegetation photosynthetic capacity***

74 Approximately 14 years (February 2000 - December 2013) of 16-day 0.05° resolution  
75 MODIS Enhanced Vegetation Index (EVI) data (MOD13C1, Collection 5) were obtained  
76 from the NASA/USGS data archive centre (<https://lpdaac.usgs.gov/>). Quality control was  
77 applied to retain high-quality observations while minimising aerosol and cloud  
78 contamination. EVI is a proxy for canopy “greenness”, which is an integrative composite  
79 property of green foliage, leaf chlorophyll content, and canopy architecture<sup>12</sup>. Annual  
80 integrated EVI (termed iEVI) has been widely used as a remote sensing surrogate of annual  
81 vegetation productivity from arid grassland to forests. In Australia, MODIS EVI has been  
82 found to be strongly correlated with eddy-covariance flux tower derived gross primary  
83 productivity (GPP)<sup>13</sup>. As an independent and more direct measure of photosynthesis, we use  
84 version 26 global monthly (level 3) solar-induced chlorophyll fluorescence (SIF) at ground  
85 footprint of 0.5°×0.5° from Sep-2007 to Dec-2014 retrieved from the Global Ozone  
86 Monitoring Experiment 2 (GOME-2) instrument. SIF is emitted by photosynthetically active  
87 chlorophyll molecules: part of the energy absorbed by chlorophyll is not used for carbon  
88 fixations, but re-emitted at longer wavelengths in the 650-800 nm spectral region<sup>14</sup>. SIF  
89 measurements from space offer an alternative means for assessing terrestrial photosynthetic  
90 activity and productivity at regional to global scales<sup>15-17</sup>. Despite its coarse-resolution (50km)  
91 at this moment, the GOME-2 SIF provides a complementary indicator of photosynthetic rate

92 of traditional spectral vegetation indices because SIF is emission instead of reflectance, thus  
93 avoids the contaminations from soil background<sup>16-18</sup>. To minimise the latitudinal and  
94 temporal variations in fluorescence retrievals due to the variations in incoming solar  
95 radiation, the SIF was normalised by the cosine of the solar zenith angle (surrogate of  
96 top-of-atmosphere solar radiation)<sup>15</sup>. The seasonality of SIF is strongly correlated with that of  
97 GPP derived from flux tower measurements<sup>17-18</sup>. It has been shown that negative SIF  
98 anomalies, particularly for croplands and grasslands, is related to drought-induced reduction  
99 in photosynthetic light-use-efficiency<sup>19</sup>.

### 100 ***1.3 In-situ measurements of net ecosystem carbon exchange by eddy-covariance flux*** 101 ***towers***

102 Eddy-covariance (EC) flux towers provide the most direct measurements of carbon fluxes  
103 between an ecosystem and the atmosphere. A full 2 years and 3 months continuous record of  
104 net ecosystem production (NEP) from Sep-2010 to Dec-2013 measured by two EC flux  
105 towers located at Australia's unique semi-arid ecosystems (refer Fig. 1g for locations of these  
106 two sites) were accessed from the OzFLUX network  
107 (<http://data.ozflux.org.au/portal/home.jsp>). The Alice Springs site is located at central  
108 Australia semi-arid Mulga woodland (MAP = 443±222 mm, 133.25°E 22.28°S)<sup>20-21</sup>, while  
109 the Calperum site is located at the southeast Australia semi-arid Mallee woodland (MAP =  
110 251±157 mm, 140.59°E 34.00°S)<sup>22</sup>. Original 30-min Level 3 data was aggregated to monthly  
111 and annual values for each site.

### 112 ***1.4 Standardised Precipitation-Evapotranspiration drought Index***

113 To characterise the extent and severity of drought, we used the global 0.5° gridded monthly  
114 Standardised Precipitation-Evapotranspiration Index (SPEI) provided by digital CSIC  
115 (Institutional Repository of the Spanish National Research Council,  
116 <http://sac.csic.es/spei/database.html>)<sup>23</sup>. SPEI takes into account both precipitation and  
117 temperature to determine drought severity and reflects the cumulative effect of the imbalance  
118 between atmospheric supply (precipitation) and demand (reference evapotranspiration).  
119 Positive SPEI indicates water-balance greater than historical median, and negative SPEI  
120 indicates water-balance less than historical median. Because the SPEI is normalised, wetter  
121 and drier climates can be represented in the same scale. The SPEI is calculated using monthly  
122 meteorological dataset from the Climatic Research Unit of the University of East Anglia

123 (CRU-TS, version 3.22) in which reference evapotranspiration was estimated using the  
124 FAO-56 Penman-Monteith equation.

### 125 ***1.5 GRACE Terrestrial Total Water Storage Change***

126 Global terrestrial total water storage change (TWSC) derived from Release-5 Level-2 Gravity  
127 Recovery and Climate Experiment (GRACE) data was obtained from NASA's Jet Propulsion  
128 Laboratory (<http://grace.jpl.nasa.gov/data/get-data/>). The GRACE mission was launched by  
129 NASA and the German Aerospace Centre (DLR) in March 2002. The system consists of twin  
130 satellites, one following the other at a distance of ~220 km, in identical Earth orbits.  
131 GRACE was designed to exploit the unique relationship between variations in the gravity  
132 field and changes in mass at the Earth's surface<sup>24</sup>. Because changes in gravity on land are  
133 mainly caused by changes in water-storage, variations of GRACE-derived total water storage  
134 (TWS) can be obtained by subtracting the monthly data from the historical mean, thus  
135 representing total water storage change (TWSC) at any given month relative to the  
136 2004-2009 baseline mean. TWSC is a good measure of vertically integrated changes in  
137 groundwater, surface water, soil moisture, snow water and biological water. For this study, an  
138 ensemble average TWSC was calculated using GRACE data processed independently by  
139 three research centres (NASA's JPL, University of Texas Center for Space Research, and  
140 Geo-Forschungs-Zentrum Potsdam). The GRACE TWSC data from July 2002 to December  
141 2014 is gridded at monthly and 1° resolution, with units of cm.

### 142 ***1.6 Gridded meteorological datasets***

143 We used high-resolution (5 km × 5 km) gridded precipitation dataset developed for the  
144 Australian Water Availability Project (AWAP)<sup>25</sup>. This dataset uses topography-resolving  
145 analysis methods applied to all available monthly precipitation data that pass a series of  
146 internal quality control tests. The temperature time series is calculated from a homogeneous  
147 temperature dataset (Australian Climate Observations Reference Network-Surface Air  
148 Temperature, or ACORN-SAT), which is developed for monitoring climate variability and  
149 change in Australia<sup>25</sup>. For global analysis, we used the global monthly 0.25° precipitation  
150 dataset provided by NOAA's Global Precipitation Climatology Centre (GPCC, version 6)<sup>26</sup>.

### 151 ***1.7 Global fire emissions database (GFED)***

152 We used the latest fourth-generation gridded ( $0.25^\circ$ ) monthly global fire emissions database  
153 (GFED4.1s) (<http://www.globalfiredata.org>)<sup>10, 27-28</sup>. Fire emissions were estimated by  
154 assimilation of satellite observations on fire activity and vegetation productivity from  
155 multiple spaceborne sensors, including MODIS burned area maps, active fire information  
156 from the Tropical Rainfall Measuring Mission (TRMM) Visible and Infrared Scanner (VIRS)  
157 and the Along-Track Scanning Radiometer (ATSR) sensors<sup>27</sup>. The primary update of GFED  
158 V4.1s as compared to previous version is the consideration of small fire burned area, as  
159 described in Randerson et al.<sup>28</sup>. Monthly fire emissions over Australia were spatially  
160 aggregated to the entire continent and temporally aggregated to each year from 2000 to 2013.  
161 Please refer Supplementary Table S1 for Australia continent-wide total fire emissions for  
162 each year.

### 163 ***1.8 Identifying very wet years***

164 To identify the precipitation pulses while taking into account the long-term trend in annual  
165 precipitation at any given location, the original time series of annual precipitation was first  
166 linearly-detrended ( $PPT_{dt}$ ). The second step calculated the standard anomaly of detrended  
167 annual precipitation ( $\sigma PPT_{dt}$ ). Then very wet years were identified when an anomaly in  
168 detrended annual precipitation for any given location and given year was equal to or greater  
169 than  $\sigma PPT_{dt}$ . The intensity for each very wet year ( $\text{mm yr}^{-1}$ ) was defined as the annual  
170 precipitation for that year. For continuous wet years, e.g., 2010-2011, we believe that these  
171 should be treated as a single very wet period since their influences on terrestrial ecosystems  
172 were in a continuous rather than discrete manner. Therefore, the intensity of continuous very  
173 wet years was calculated as the mean of annual precipitation for the period of continuous  
174 very wet years (e.g., mean of 2010 and 2011). The linear trend of precipitation of very wet  
175 years from 1900 to 2013 was then calculated for each grid cell across the entity of Australia.  
176 *Supplementary Fig. S6* shows a graphical illustration of the steps for identifying very wet  
177 years. Significant tests were applied and only linear trends with  $p < 0.05$  are retained for  
178 further analysis.

### 179 ***1.9 Vegetation map***

180 We used the Australian Major Vegetation Group (MVG) dataset provided by National  
181 Vegetation Information System (NVIS, v4.1)<sup>29</sup>. To understand biome-level contribution to  
182 carbon sink anomaly, we grouped 26 NVIS major vegetation groups into five biomes: forest,

183 savanna, shrubland, grassland, and agriculture. The forest biome includes rainforest and  
 184 closed forests. The savanna biome, the tree-shrub-grass multi-strata system, includes all open  
 185 forests, woodlands, as well as parts of shrublands, with both *Eucalyptus*, *Acacia* or other trees  
 186 as dominant canopy species<sup>30</sup>. The grassland biome includes hummock grassland, tussock  
 187 grassland, and other grassland types. The agricultural biome includes cropland and pastures.

## 188 2. Supplementary table and figures

189 **Supplementary Table S1.** Summary of Australia’s continental-aggregated annual NEP,  
 190 precipitation, temperature, SPEI, NEP, EVI, SIF, and fire emission for each hydrological year  
 191 (September-August) from 2000-01 to 2012-03. Total NEP is computed using all pixels from  
 192 Australia (7.69 million km<sup>2</sup>).

Year	P (mm yr-1)	T (°C)	SPEI	Total NEP (Pg C yr-1)	NEP per unit area (g C m-2 yr-1)	EVI	SIF	Fire Emission (Pg C yr-1)
2000-01	606	21.72	0.42			0.18		0.16
2001-02	420	21.61	-0.13			0.17		0.16
2002-03	409	22.29	-0.49			0.16		0.17
2003-04	511	21.98	0.20			0.18		0.08
2004-05	379	22.42	-0.58			0.16		0.13
2005-06	539	21.93	0.46			0.18		0.07
2006-07	450	22.31	-0.23			0.17		0.14
2007-08	443	21.92	-0.32			0.17	0.38	0.10
2008-09	509	22.26	0.13			0.17	0.38	0.07
2009-10	545	22.26	0.10			0.17	0.39	0.10
2010-11	792	21.26	1.14	0.97	126.14	0.19	0.46	0.07
2011-12	567	21.30	0.38	0.48	62.42	0.18	0.41	0.17
2012-13	422	22.69	-0.38	0.08	10.40	0.16	0.34	0.14
Mean±1 σ	507±110	22.00±0.43	0.05±0.48	0.51±0.44	66.32±57.97	0.17±0.01	0.39±0.04	0.12±0.04

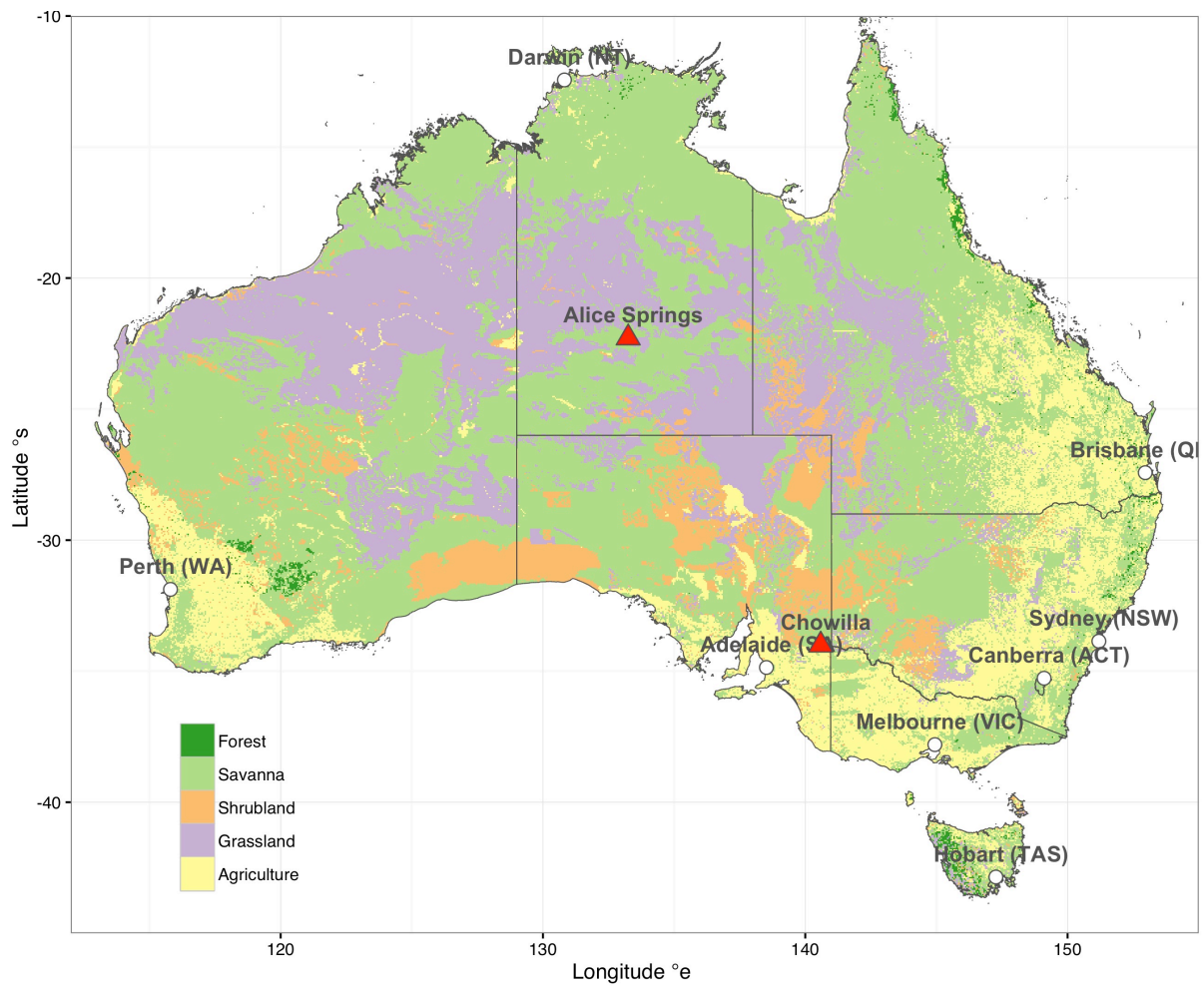
193 P: anomaly of annual precipitation relative to the average of 1970-2013 (mm yr<sup>-1</sup>); T: anomaly of annual average  
 194 temperature relative to the average of 1970-2013 (°C); SPEI: Standardised Precipitation-Evapotranspiration  
 195 Index; NEP: Net Ecosystem Production; EVI: annual average MODIS EVI; SIF: annual average GOME-2 SIF;  
 196 Fire Emission : annual fire carbon emission from GFED.

197

198 **Supplementary Table S2.** Summary of climatology, percentage contribution of each biome  
 199 to Australia's terrestrial primary productivity anomaly (surrogated by MODIS EVI anomaly),  
 200 as well as mean rain-use-efficiency (RUE) of each biome during the 2010-2011 La Niña wet  
 201 period. Mean RUE for each biome was calculated as biome-level average of the ratio  
 202 between EVI anomaly and rainfall anomaly in 2010-11.

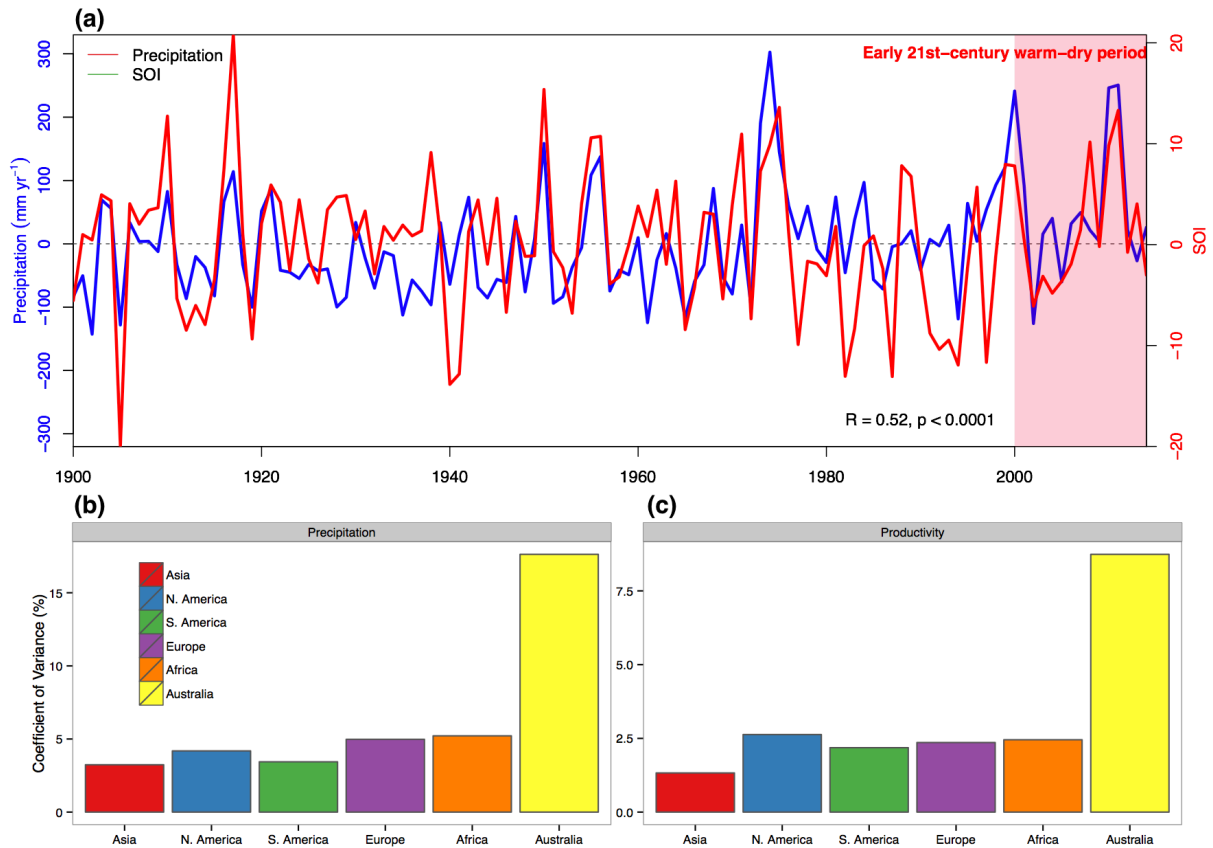
<b>Biome</b>	<b>Area (million km<sup>2</sup>)</b>	<b>Percentage Coverage (%)</b>	<b>MAP (mm)</b>	<b>MAT (°C)</b>	<b>Contribution to 2010-11 terrestrial primary productivity (MODIS EVI) (%)</b>	<b>Mean RUE±1σ (EVI per 100 mm of rainfall)</b>
<b>Forest</b>	0.05	0.65	1267	16.34	1	0.0030 ± 0.0072
<b>Savanna</b>	3.94	51.08	541	22.34	46	0.0074 ± 0.0071
<b>Shrubland</b>	0.57	7.60	249	20.62	11	0.0128 ± 0.0082
<b>Grassland</b>	1.95	24.83	398	24.36	24	0.0086 ± 0.0074
<b>Agriculture</b>	1.16	15.83	573	18.87	19	0.0109 ± 0.0082

203 MAP: mean annual precipitation; MAT: mean annual temperature.



205

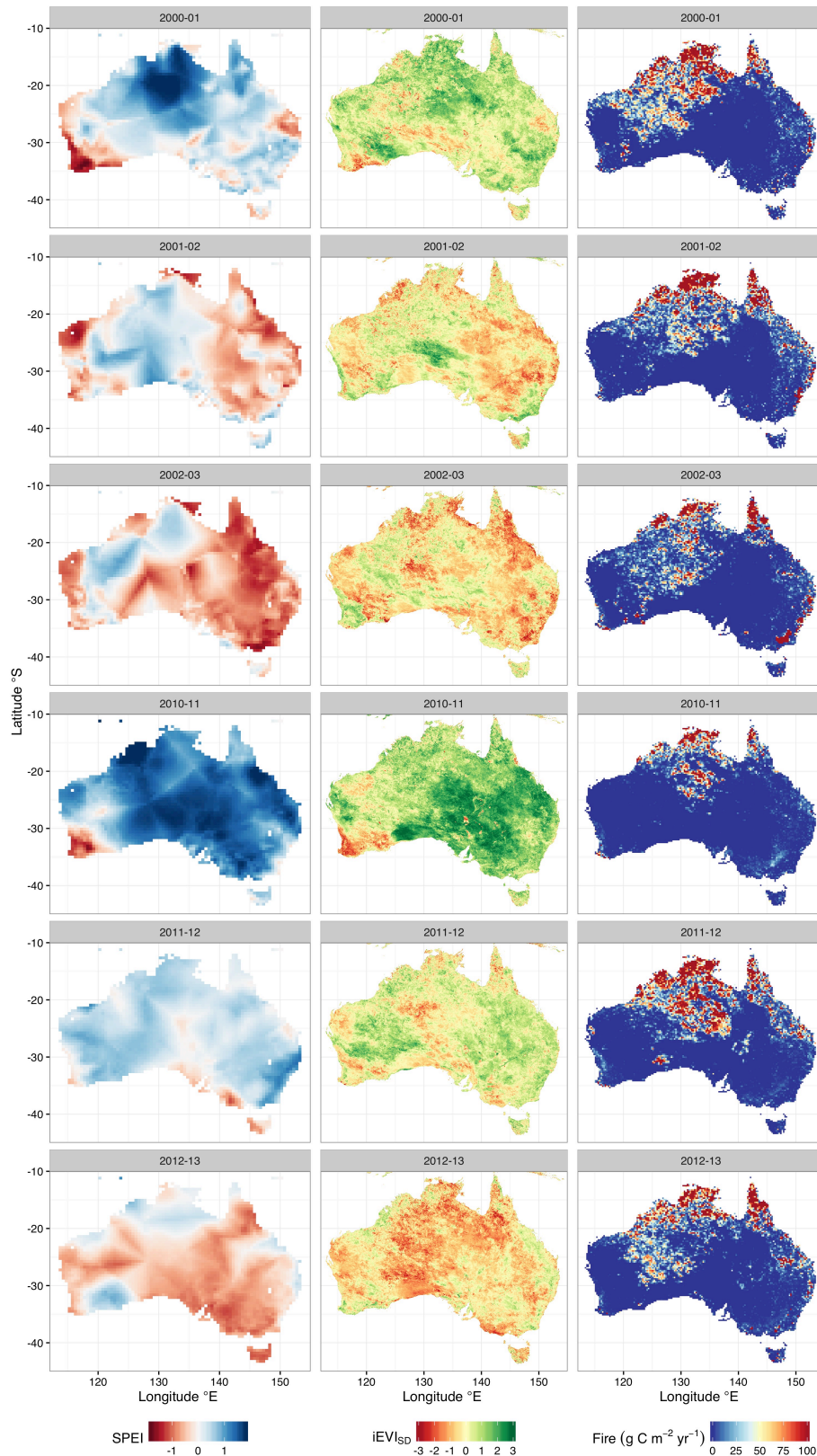
206 **Supplementary Figure S1.** Map of Australia's biome types. Classification of Australia's  
 207 ecosystems into biome types using Major Vegetation Group map provided by Australian  
 208 National Vegetation Information System (NVIS, v4.1). Australia's major cities are labelled as  
 209 white solid circles, while red solid triangles are two eddy-covariance (EC) flux tower sites  
 210 located in central and south-east Australia, providing ground measurements of net ecosystem  
 211 carbon exchange for verifying the 'top-down' estimates. Map was drawn using R version  
 212 3.1.2 (<http://www.r-project.org/>).



213

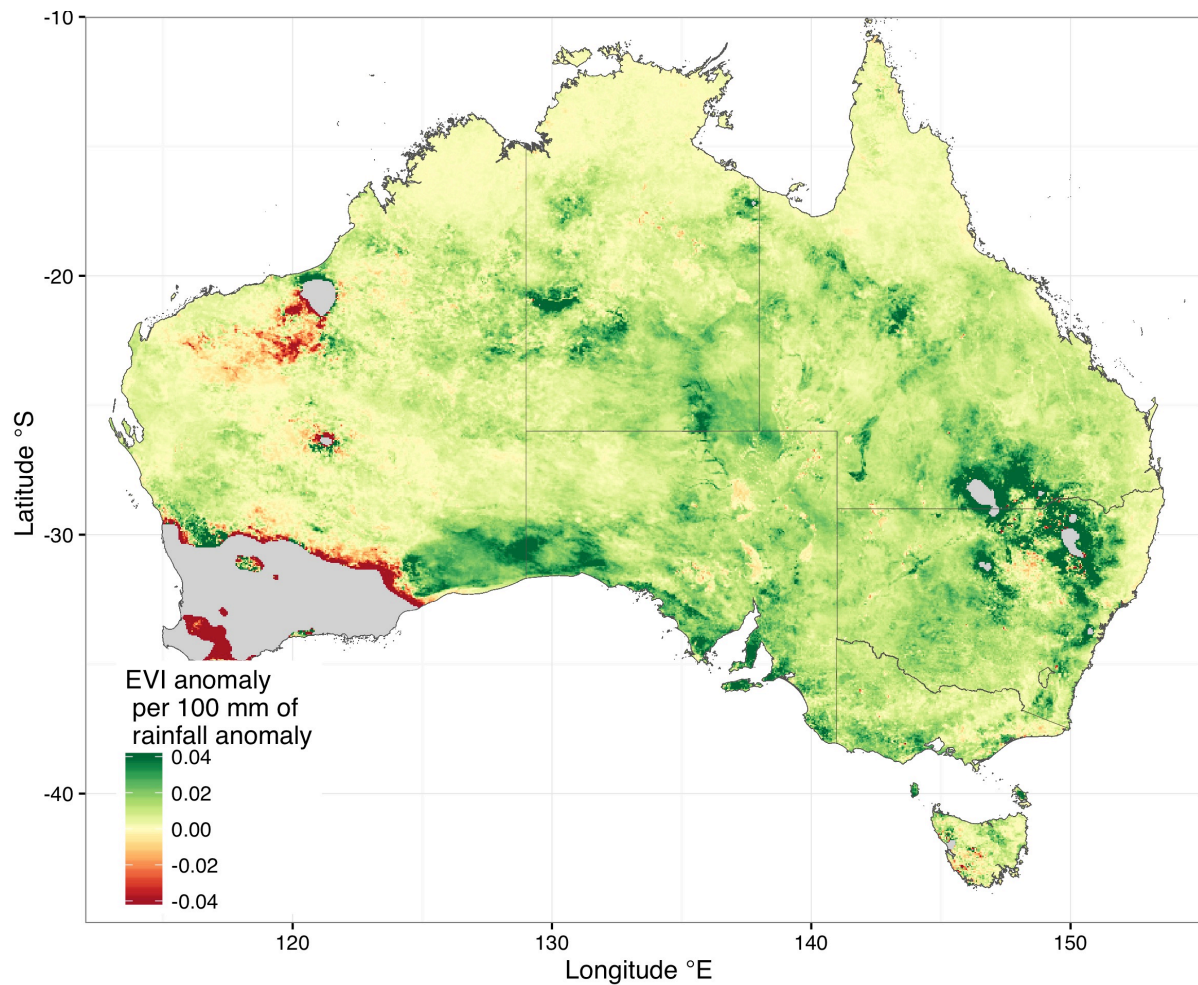
214 **Supplementary Figure S2.** Inter-annual variance of Australia's precipitation. (a) Variations  
 215 in annual precipitation anomaly averaged across the entirety of Australia alongside the  
 216 Southern Oscillation Index (SOI) from 1900 to 2014; (b) Coefficient of variance (%) in  
 217 annual precipitation and annual vegetation productivity of six continents. Inter-annual  
 218 variance is represented by coefficient of variance (CV, %). Global precipitation data is from  
 219 NOAA Global Precipitation Climatology Centre (GPCC, v6). Yearly integrated MODIS  
 220 Enhanced Vegetation Index (EVI) is used as a proxy for vegetation productivity. Reference  
 221 period: 2000-2014. SOI data is obtained from Bureau of Meteorology, Australia.

222



223

224 **Supplementary Figure S3.** Biogeographic patterns in SPEI, iEVI (standardised anomaly)  
 225 and SIF (standardised anomaly), as well as fire carbon emission over Australia for the  
 226 2000-01 to 2002-03 and 2010-11 to 2012-13 time periods respectively. Noted that 2000-01  
 227 represents a hydrological year starting from September-2000 to August-2001. Maps were  
 228 drawn using R version 3.1.2 (<http://www.r-project.org/>).



229

230 **Supplementary Figure S4.** Spatial variations in the ratio between EVI anomaly and rainfall  
 231 anomaly during the 2010-11 La Niña wet period. This map indicates the variations in

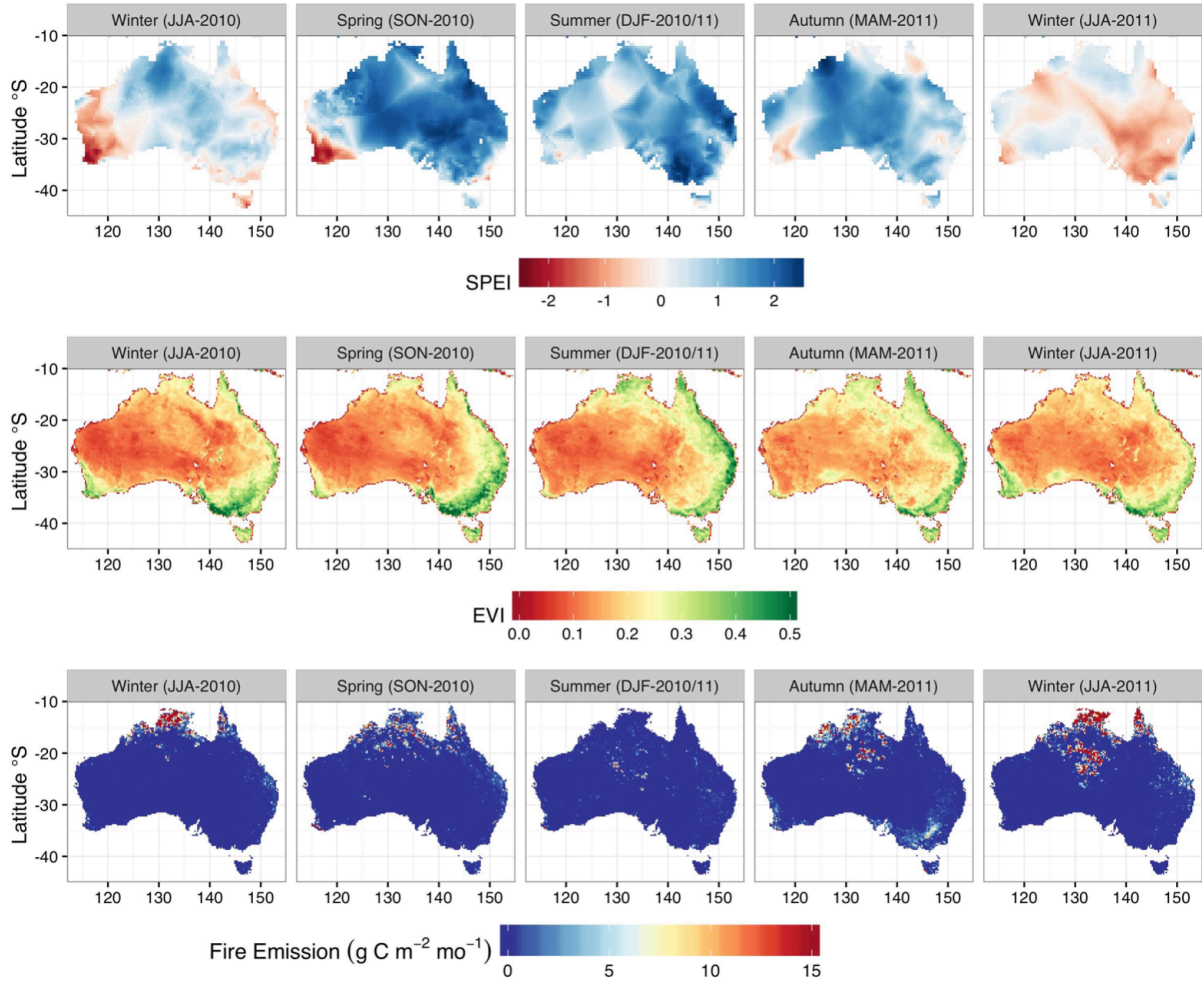
232 efficiency of vegetation in using rainfall for generating productivity anomaly across space.

233 Areas with negative rainfall anomaly in 2010-11 were shown in grey. Areas with negative

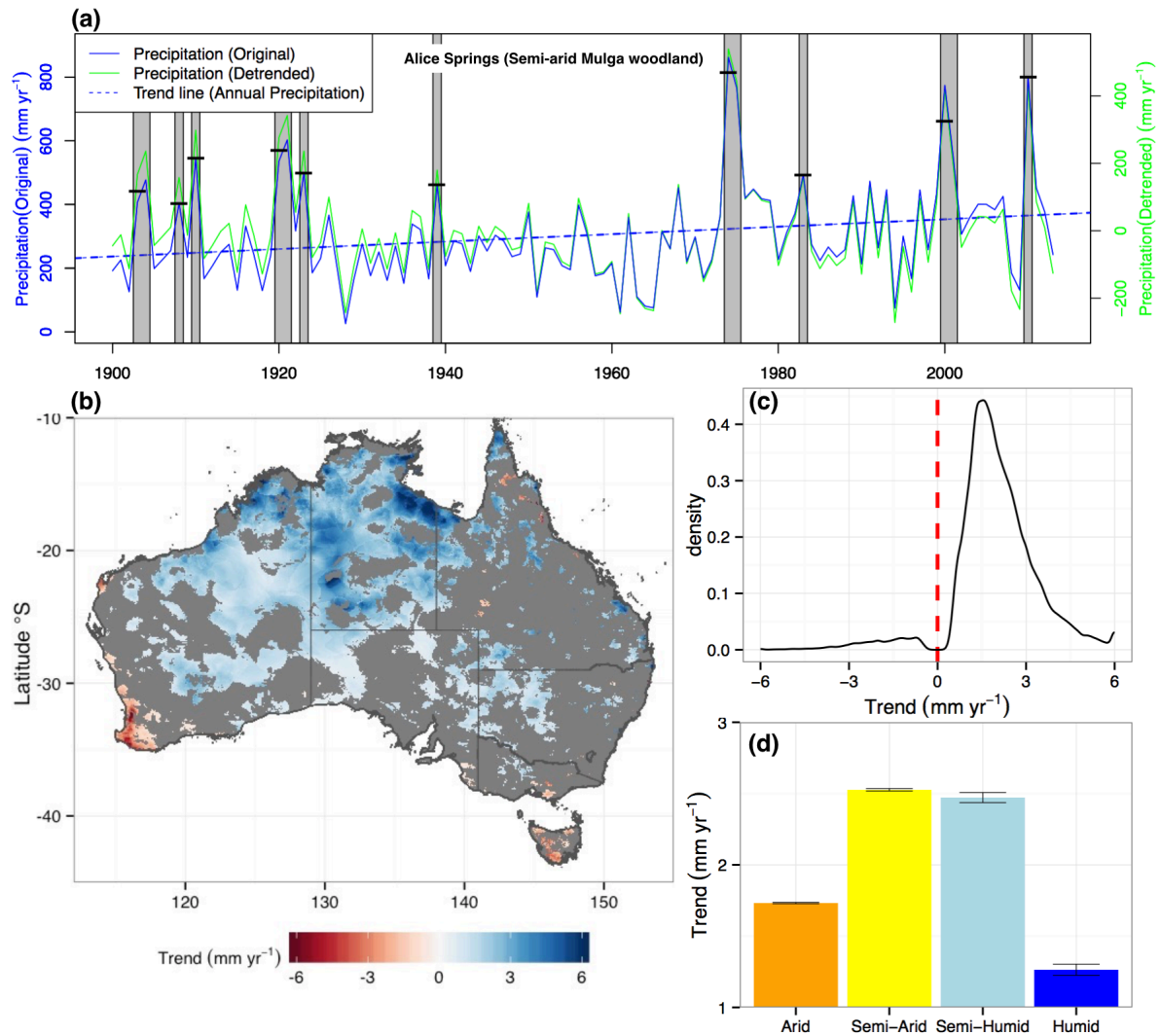
234 ratio between EVI anomaly and rainfall anomaly indicate ecosystems that showed a decline

235 in vegetation productivity given a wet pulse in 2010-11. Map was drawn using R version

236 3.1.2 (<http://www.r-project.org/>).



237 **Supplementary Figure S5.** Seasonal variations in SPEI, EVI, and fire emission for the  
238 2010-11 wet period. The five panels show seasons from Austral winter (June-August, 2010),  
239 spring (September-November, 2010), summer (December-2010 to February-2011), autumn  
240 (March-May, 2011), and winter (June-August, 2011). Maps were drawn using R version 3.1.2  
241 (<http://www.r-project.org/>).  
242  
243

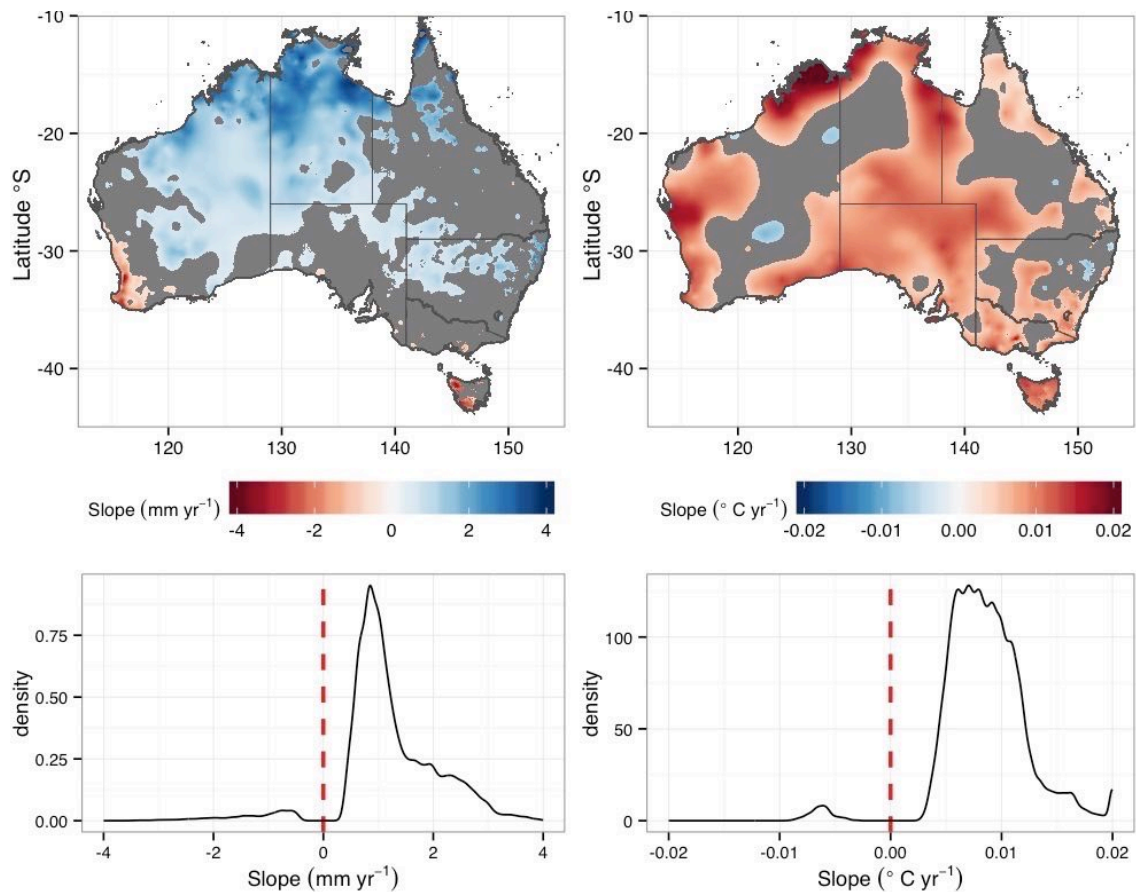


244

245 **Supplementary Figure S6.** Trend in precipitation amounts during the very wet years across  
 246 Australia from 1900s to 2013. (a) A graphical illustration of the method for identifying very  
 247 wet years using long-term annual precipitation data from one meteorological station; (b)  
 248 map of the trend in precipitation amounts during the very wet years from 1900 to 2013 over entire  
 249 Australia. Grey areas indicate pixels without significant trend ( $p < 0.05$ ) detected; (c)  
 250 distribution of the trend in precipitation amounts during the very wet years across Australia;  
 251 (d) zonal average of trend in precipitation amounts during the very wet years by climatic  
 252 zones over Australia. Map was drawn using R version 3.1.2 (<http://www.r-project.org/>).

253

254



255

256 **Supplementary Figure S7.** Trend in precipitation and temperature across Australia from  
 257 1900s to 2013. For both annual precipitation (left) and annual mean daily temperature (right),  
 258 the trend is expressed as the slope of linear regression model, with the unit of  $\text{mm yr}^{-1}$  for  
 259 precipitation and  $^{\circ}\text{C yr}^{-1}$  for temperature, respectively. Grey areas indicate the pixels without  
 260 a significant trend ( $p < 0.05$ ). Below panels show the empirical probability density function  
 261 plots for significant trend of precipitation ( $p < 0.05$ ) and significant trend of temperature ( $p <$   
 262  $0.05$ ) over Australia respectively. Maps were drawn using R version 3.1.2  
 263 (<http://www.r-project.org/>).

### 264 3. Supplementary references

- 265 1. Peylin, P. *et al.* Global atmospheric carbon budget: results from an ensemble of atmospheric  
 266  $\text{CO}_2$ -inversions. *Biogeosci* **10**, 6699–6720 (2013).
- 267 2. Crisp, D. *et al.* The ACOS  $\text{CO}_2$  retrieval algorithm; Part II: Global  $\text{XCO}_2$  data characterization.  
 268 *Atmos Meas Tech* **5**, 687–707 (2012).
- 269 3. Houweling, S. *et al.* An intercomparison of inverse models for estimating sources and sinks of  $\text{CO}_2$   
 270 using GOSAT measurements. *J Geophys Res A* **120**, 5253–5266 (2015).
- 271 4. Yokota, T. *et al.* Global Concentrations of  $\text{CO}_2$  and  $\text{CH}_4$  Retrieved from GOSAT: First Preliminary  
 272 Results. *Sola* **5**, 160–163 (2009).
- 273 5. Chevallier, F. *et al.*  $\text{CO}_2$  surface fluxes at grid point scale estimated from a global 21-year  
 274 reanalysis of atmospheric measurements. *J Geophys Res* **115**, D21307 (2010).
- 275 6. Chevallier, F. On the statistical optimality of  $\text{CO}_2$  atmospheric inversions assimilating  $\text{CO}_2$  column  
 276 retrievals. *Atmos Chem Phys* **15**, 11133–11145 (2015).

- 277 7. Chevallier, F. *et al.* Climate Assessment Report for the GHG-CCI project of ESA's Climate  
278 Change Initiative, pp.87, version 2, 22 April 2015.
- 279 8. Locatelli, R. *et al.* Atmospheric transport and chemistry of trace gases in LMDz5B: evaluation and  
280 implications for inverse modelling. *Geosci Model Dev* **8**, 129–150 (2015).
- 281 9. Krinner, G. *et al.* A dynamic global vegetation model for studies of the coupled  
282 atmosphere-biosphere system. *Global Biogeochem Cy* **19**, GB1015 (2005).
- 283 10. van der Werf, G. R. *et al.* Global fire emissions and the contribution of deforestation, savanna,  
284 forest, agricultural, and peat fires (1997–2009). *Atmos Chem Phys* **10**, 11707–11735 (2010).
- 285 11. Chevallier, F. *et al.* Contribution of the Orbiting Carbon Observatory to the estimation of CO<sub>2</sub>  
286 sources and sinks: Theoretical study in a variational data assimilation framework. *J Geophys Res* **112**,  
287 D09307 (2007).
- 288 12. Huete, A. R. *et al.* Overview of the radiometric and biophysical performance of the MODIS  
289 vegetation indices. *Remote Sens Environ* **83**, 195–213 (2002).
- 290 13. Ma, X. *et al.* Parameterization of an ecosystem light-use-efficiency model for predicting savanna  
291 GPP using MODIS EVI. *Remote Sens Environ* **154**, 1–19 (2014).
- 292 14. Baker, N. R. Chlorophyll Fluorescence: A Probe of Photosynthesis In Vivo. *Annu Rev Plant Biol*  
293 **59**, 89–113 (2008).
- 294 15. Joiner, J. *et al.* Global monitoring of terrestrial chlorophyll fluorescence from  
295 moderate-spectral-resolution near-infrared satellite measurements: methodology, simulations, and  
296 application to GOME-2. *Atmos Meas Tech* **6**, 2803–2823 (2013).
- 297 16. Guanter, L. *et al.* Global and time-resolved monitoring of crop photosynthesis with chlorophyll  
298 fluorescence. *Proc Natl Acad Sci USA* **111**, E1327–33 (2014).
- 299 17. Joiner, J. *et al.* The seasonal cycle of satellite chlorophyll observations and its relationship to  
300 vegetation phenology and ecosystem-atmosphere carbon exchange. *Remote Sens Environ* **152**,  
301 375–391 (2014).
- 302 18. Parazoo, N. C. *et al.* Terrestrial gross primary production inferred from satellite fluorescence and  
303 vegetation models. *Glob Change Biol* **20**, 3103–3121 (2014).
- 304 19. Yoshida, Y. *et al.* The 2010 Russian drought impact on satellite measurements of solar-induced  
305 chlorophyll fluorescence: Insights from modeling and comparisons with parameters derived from  
306 satellite reflectances. *Remote Sens Environ* **166**, 163–177 (2015).
- 307 20. Eamus, D. *et al.* Carbon and water fluxes in an arid-zone Acacia savanna woodland: An analyses  
308 of seasonal patterns and responses to precipitation events. *Agr Forest Meteorol* **182**, 225–238 (2013).
- 309 21. Cleverly, J. *et al.* Dynamics of component carbon fluxes in a semi-arid Acacia woodland, central  
310 Australia. *J Geophys Res G* **118**, 1168–1185 (2013).
- 311 22. Meyer, W. S., Kondrlovà, E. & Koerber, G. R. Evaporation of perennial semi-arid woodland in  
312 southeastern Australia is adapted for irregular but common dry periods. *Hydrol Process* **29**,  
313 3714–3726 (2015).
- 314 23. Vicente-Serrano, S. M., Beguería, S., López-Moreno, J. I. A multiscalar drought index sensitive to  
315 global warming: The standardized precipitation evapotranspiration index. *J Clim* **23**, 1696–1718  
316 (2010).
- 317 24. Wahr, J., Swenson, S., Zlotnicki, V. & Velicogna, I. Time-variable gravity from GRACE: First  
318 results. *Geophys Res Lett* **31**, L11501–4 (2004).
- 319 25. Jones, D. A., Wang, W. & Fawcett, R. High-quality spatial climate data-sets for Australia. *Aust*  
320 *Meteorol Ocean* **58**, 233–248 (2009).
- 321 26. Schneider, U., Becker, A., Meyer-Christoffer, A., Ziese, M. & Rudolf, B. Global precipitation  
322 analysis products of the GPCC. *Global Precipitation Climatology Centre (GPCC), DWD, Internet*

- 323 *Publikation*, **112** (2008).
- 324 27. Giglio, L., Randerson, J. T., & Werf, G. R. Analysis of daily, monthly, and annual burned area  
325 using the fourth - generation global fire emissions database (GFED4). *J Geophys Res G*, **118**, 317 -  
326 328 (2013).
- 327 28. Randerson, J. T., Chen, Y., van der Werf, G. R., Rogers, B. M., & Morton, D. C. Global burned  
328 area and biomass burning emissions from small fires. *J Geophys Res A*, **117**, G04012 (2012).
- 329 29. NVIS. Australia's native vegetation - A summary of Australia's major vegetation groups (2007).
- 330 30. Huntley, B. J. & Walker, B. H. Ecology of tropical savannas. Vol. 42. Springer-Verlag  
331 Berlin-Heidelberg (1982).